AN APPROACH TO THE CONSTRAINED DESIGN OF NATURAL LAMINAR FLOW AIRFOILS

by

Bradford Earl Green

B.S. Aerospace Engineering,

Embry-Riddle Aeronautical University, April, 1993

A Thesis submitted to

The Faculty of

The School of Engineering and Applied Science of

The George Washington University

in partial satisfaction of the requirements for the degree of

Master of Science

July 1995

This research was conducted at NASA Langley Research Center

Abstract

A design method has been developed by which an airfoil with a substantial amount of natural laminar flow can be designed, while maintaining other aerodynamic and geometric constraints. After obtaining the initial airfoil's pressure distribution at the design lift coefficient using an Euler solver coupled with an integral turbulent boundary layer method, the calculations from a laminar boundary layer solver are used by a stability analysis code to obtain estimates of the transition location (using N-Factors) for the starting airfoil. A new design method then calculates a target pressure distribution that will increase the laminar flow toward the desired amount. An airfoil design method is then iteratively used to design an airfoil that possesses that target pressure distribution. The new airfoil's boundary layer stability characteristics are determined, and this iterative process continues until an airfoil is designed that meets the laminar flow requirement and as many of the other constraints as possible.

Table of Contents

List of Tables

List of Figures

List of Symbols

A	relaxation factor for N-Factor design method
C	surface curvature of airfoil, $\hat{C}/c$
C_p	pressure coefficient, $(p - p_\infty)/q_\infty$
c	chord length (ft)
c_d	section drag coefficient, $d/(q_\infty c)$
c_l	section lift coefficient, $l/(q_\infty c)$
c_m	pitching moment coefficient, $(l\hat{x})/\left(q_\infty c^2\right)$
c_w	phase speed of Tollmien-Schlichting waves (ft/s)
d	section drag (lb_f)
F	pressure gradient parameter, Equation 11
G	scale factor for linear scaling method
l	section lift (lb_f)
M	Mach number, $U/\sqrt{\gamma \cdot R \cdot T}$
N	N-Factor, Equation 16
n_f	number of frequencies
p	static pressure (lb_f/ft^2)
q	dynamic pressure, $\frac{1}{2}\rho U^2$
R	gas constant (lb_f-ft/slugs·R)

Re	free-stream Reynolds number based on chord, $(\rho_\infty U_\infty c)/\mu_\infty$
r_{le}	leading-edge radius, $\hat{r}_{le}/c$
s	chordwise distance from stagnation point, Equation 42
T	static temperature (R)
t	airfoil thickness, $\hat{t}/c$
U	local velocity (ft/s)
$\vec{V}_g$	complex group velocity (ft/s)
v_w	velocity of Tollmien-Schlichting waves (ft/s)
W	weighting function for weighted averaging technique
X	equivalent flat plate distance, Equation 1
x	distance along chord of airfoil, $\hat{x}/c$
y	vertical distance of airfoil, $\hat{y}/c$

Greek

α	angle of attack (degrees)
γ	ratio of specific heats
δ	thickness of turbulent boundary layer, Equation 8
δ^*	displacement thickness of turbulent boundary layer, Equation 10
ζ, ξ	wave numbers (1/ft)
θ	momentum thickness of turbulent boundary layer, Equation 9
κ	relaxation factor for turbulent boundary layer
λ	relaxation factor used to meet lift constraint

μ	kinematic viscosity (slugs/(ft-s))
ρ	density (slugs/ft^3)
σ	arc length along surface of airfoil (ft)
ς	relaxation factor used to meet pitching moment constraint
τ	parameter for airfoil design method
ϕ_{te}	trailing-edge angle (degrees)
ψ	wave angle (degrees)
ω	frequency (1/s)

Subscript

a	analysis
av	average
cp	control point
crit	critical
des	design
e	effective
i	imaginary
j	airfoil station
l	lower surface
max	maximum
min	minimum
r	real

stag	stagnation point
T	target
tol	tolerance
tr	transition
u	upper surface
∞	free-stream conditions

Superscript

i	iteration index
*	sonic conditions, $M = 1$
^	dimensional quantity

Acknowledgments

I would like to first of all thank Dr. James Luckring for giving me the opportunity to perform this research in the Transonic/Supersonic Aerodynamics Branch at NASA Langley Research Center. In addition, I greatly appreciate the help that I received from my research advisors Mr. Richard Campbell and Dr. Ray Mineck, without whom I would not have gotten so far, so fast. Thanks for all of those times when you spared 10 minutes of your time, even though you didn't have one. I also wish to thank my academic advisor, Dr. John Whitesides of the George Washington University, for his guidance.

Furthermore, I would like to thank my two sisters, Leah Ann and Tee-Tea, for their support. Thanks for always giving me a place to call home. I also would like to thank my roommate Glenn for his support, and for always making coming home fun.

To the Memory of my Parents,

Earl and Joanne Green

1.0 Introduction

Since Orville Wright first flew in December of 1903, there have been considerable attempts to find methods to reduce the drag of airplanes. A reduction in drag means that airplanes can operate more efficiently by using less fuel, which results in lower operating costs and smaller, quieter engines. Also with the reduction in fuel consumption comes the ability to produce aircraft with longer ranges and bigger payloads.

In the 1930's, it was found that longer runs of laminar flow over an airfoil resulted in a lower profile drag and that favorable pressure gradients contributed to prolonged laminar boundary layers (ref. 1). Using these ideas, pressure distributions having the pressure minimum located near the position of desired transition were sought. Once the desired pressure distribution was found, an airfoil with that pressure distribution was then derived, using theoretical techniques such as Theodorsen's method (ref. 2), and tested. The NACA 1-6 series airfoils are examples of airfoils that were designed in this manner (ref. 3). This was the birth of attempts to achieve long runs of natural laminar flow (NLF) to reduce airplane drag.

In the 1960's, a new method for creating long runs of laminar flow was utilized. Now called laminar flow control (LFC), this method achieved laminar flow through suction holes located at selected spanwise stations on the wing. There are two results of boundary layer suction. First of all, boundary layer suction thins the boundary layer and lowers the effective Reynolds number. Secondly, boundary layer suction changes the boundary layer profiles. The changes that result contribute to boundary layer stability, which results in longer runs of laminar flow (ref. 4). Since then, this technology has been further researched and several airfoils using LFC have been developed (refs. 5,6).

Although the benefits of LFC are tremendous, especially in three-dimensional flows, the physical application of an LFC system to a wing causes several problems. One problem is the increased weight that the system adds to the airplane. Since the aircraft weight is increased, a trade-off must be made to get the true benefits of the LFC system. Another problem of LFC is contamination from insects and icing. Often times, insect remains or ice on the surface trip the boundary layer, reducing the efficiency of the LFC system. Another possible problem arises if a mechanical failure occurs and the system on one wing does not work properly. In this case, lift will be lost on the wing and its drag will increase, causing unwanted rolling and yawing moments. If these problems with LFC systems can be overcome, perhaps the true benefits of the technology can be experienced.

Within the past fifteen years, due to the advances of the modern-day computer, even more research has gone into the benefits of and the methods for achieving NLF. Although most of this research has been applied to designing airfoils (refs. 7-11), some research has been done on designing fuselages for NLF (refs. 12-14). The methods implemented for designing airfoils with long runs of NLF seem to be mainly trial and error methods using linear stability theory to assess the effect of changing the pressure distribution, although there have been some optimization methods developed for axisymmetric airplane elements (ref. 12). Thus, the design methods employed for modifying airfoil pressure distributions often required extensive knowledge and experience.

In this paper, a constrained design method is presented for modifying an airfoil's shape such that long runs of NLF can be achieved. The design method uses an Euler solver coupled with an integral turbulent boundary layer method and a laminar boundary layer solver to calculate the velocity and temperature profiles at each airfoil station. A boundary layer stability analysis code is then used to find the stability of the boundary layer in terms of N-

factors, which are the logarithmic amplification of the Tollmien-Schlichting (T-S) waves. After calculating a target N-Factor distribution that forces transition to occur at the desired location, a new method is used to calculate a target pressure distribution that is closer to meeting the NLF constraints, while maintaining several aerodynamic and geometric constraints. Once the new target pressure distribution is calculated, an airfoil design method is used to design an airfoil that has that pressure distribution. This process is iterated until an airfoil is designed that meets the desired NLF, aerodynamic and geometric constraints.

2.0 Overview of the Airfoil Design Method

The flowchart shown in Figure 1 demonstrates the process by which the final NLF airfoil is iteratively designed. The first module on the flowchart uses the Euler solver discussed in Section 2.1 and the turbulent boundary layer method discussed in Section 2.2 to calculate the pressure distribution of the current airfoil. This pressure distribution is then analyzed by the laminar boundary layer solver discussed in Section 2.3 to calculate the boundary layer velocity and temperature profiles. The stability analysis code discussed in Section 2.4 then uses this data to calculate the N-Factor distribution for the current airfoil and pressure distribution. Using the current N-Factors and pressures, the Target Pressure Design module, which is discussed in Chapter 3, calculates a target pressure distribution, from which an airfoil can be designed using the flow solver and the airfoil design method discussed in Section 2.5. However, the target pressures often need to be modified while designing the new airfoil. These modifications are made by the Modify Target Pressures to Enforce Constraints module, which is discussed in Chapter 4.

Chapter 5 is included to show some results of the NLF airfoil design method. Airfoils were designed for glider, commuter and subsonic transport aircraft, which covers a wide range of Mach numbers, Reynolds numbers, and airfoil thicknesses.

While Chapters 3 and 4 discuss the newly developed components used in this project, the current chapter is devoted to discussing the existing codes that have been coupled together to design new NLF airfoils. The computer used was a Silicon Graphics Indigo2 workstation with an R4000 processor; all CPU times mentioned pertain to this computer.

2.1 Euler Solver

The Euler solver used is called GAUSS2 (General purpose Approximate factorization Upwind Scheme with Shock fitting, 2-Dimensional version), and was written by Peter

Hartwich (refs. 15-17). The code solves the two-dimensional, compressible, non-conservative Euler equations on a structured mesh.

GAUSS2 uses an upwind method that constructs a finite-difference scheme based on the theory of characteristics. Since the upwinding technique used is the non-conservative split-coefficient matrix (SCM) method, the code is fast and efficient. The dependent variables used are the speed of sound, and the two Cartesian velocity components, all of which are required in any upwind scheme. Entropy is chosen as the fourth dependent variable, which reduces the energy equation to a simple convection equation.

Away from shocks, fully one-sided, second-order accurate spatial differences are used to update the solution. The shocks are resolved using a floating shock fitting method that allows the shock to float between two grid points. Across the shock, the Rankine-Hugoniot relations are explicitly used to update the solution using the speed of sound and entropy variables.

The solution is advanced in time using a time-implicit operator containing block-tridiagonal matrices for the two-dimensional Euler equations. For calculating transient flows, the second-order accurate Crank-Nicholson time differencing is used. For the steady-state calculations used in this study, the first-order accurate Euler-backward time discretization is used due to the quick convergence rate that results from its better damping properties.

As mentioned previously, GAUSS2 is a fast flow solver. Typically only 500 CPU seconds are required to calculate the pressure distribution of the initial airfoil at the design lift coefficient.

As shown in Figure 1, GAUSS2 must also be used each time that the airfoil design method is used to design a new airfoil. Typically, only 60 iterations through the airfoil

design method are needed to design an airfoil that possesses the desired target pressures. Approximately 500 CPU seconds are required to complete these 60 iterations.

Required inputs for GAUSS2 include the current airfoil, the angle of attack, and the free-stream Mach number. Outputs of the solver include the pressure distribution on the surface of the airfoil, the location of any shocks on either surface, and the wave drag associated with these shocks.

2.2 Turbulent Boundary Layer Method

The compressible turbulent boundary layer method used is a modified version of the integral method developed by Stratford and Beavers (ref. 18). The following seven equations are taken from reference 18. With M being the local Mach number, an equivalent flat plate distance is defined as

$$X = \left(\frac{1 + 0.2M^2}{M}\right)^4 \int_0^x \left(\frac{M}{1 + 0.2M^2}\right)^4 dx \tag{1}$$

This distance represents the length over which a boundary layer growing on a flat plate would acquire the same thickness as the real boundary layer at that given location and Mach number (ref. 19).

For free-stream Reynolds numbers Re between 1 and 10 million, the method expresses the boundary layer thickness as

$$\delta = 0.37X^{0.80}Re^{-0.20}, \tag{2}$$

the momentum thickness as

$$\theta = 0.036\left(1 + 0.10M^2\right)^{-0.70}X^{0.80}Re^{-0.20}, \tag{3}$$

and the displacement thickness as

$$\delta^* = 0.046\left(1 + 0.80M^2\right)^{0.44} X^{0.80} Re^{-0.20} \tag{4}$$

For free-stream Reynolds numbers between 10 and 100 million, the method uses the following relations:

$$\delta = 0.23X^{0.833} Re^{-0.167} \tag{5}$$

$$\theta = 0.022\left(1 + 0.10M^2\right)^{-0.70} X^{0.833} Re^{-0.167} \tag{6}$$

$$\delta^* = 0.028\left(1 + 0.80M^2\right)^{0.44} X^{0.833} Re^{-0.167} \tag{7}$$

In order to find expressions for the preceding equations that are a good approximation throughout the entire range of Reynolds numbers, the equations above have been modified. The expressions used in the current application of the boundary layer method are

$$\delta = 0.276X^{0.82} Re^{-0.18} \tag{8}$$

$$\theta = 0.027\left(1 + 0.10M^2\right)^{-0.70} X^{0.82} Re^{-0.18} \tag{9}$$

$$\delta^* = 0.034\left(1 + 0.80M^2\right)^{0.44} X^{0.82} Re^{-0.18} \tag{10}$$

The original method of Stratford and Beavers does not include a calculation of the viscous drag. As a result, the method of Squire and Young (ref. 20) is used for this purpose and is implemented after calculating the characteristics of the turbulent boundary layer as described above. This method extrapolates the momentum thickness at the trailing-edge of the airfoil to infinity.

In addition, the original method of Stratford and Beavers does not include a criterion for predicting the location of turbulent separation. Therefore, the method of reference 19 is included for this reason. This method is based on the pressure gradient parameter

$$F = C_p\left(X\frac{dC_p}{dx}\right)^{1/2}\left(10^{-6}XRe\right)^{-0.10}, \tag{11}$$

where X was defined in Equation 1.

The displacement thicknesses calculated using Equation 10 are used to calculate an effective airfoil to account for viscous effects. With j being the airfoil station, the upper surface of the effective airfoil is calculated using the relation

$$y_{e,j,u} = y_{j,u} + \kappa(\delta^*)^{i}_{j,u} + (1-\kappa)\,(\delta^*)^{i-1}_{j,u}, \tag{12}$$

where $y_{e,j,u}$ is the upper surface of the effective airfoil, $y_{j,u}$ is the upper surface of the current airfoil, κ is a relaxation factor (typically 0.80), and $(\delta^*)^{i-1}_{j,u}$ and $(\delta^*)^{i}_{j,u}$ are the upper surface displacement thicknesses of the previous and current iterations, respectively. To calculate the lower surface of the effective airfoil, the relation implemented is

$$y_{e,j,l} = y_{j,l} - \kappa(\delta^*)^{i}_{j,l} - (1-\kappa)\,(\delta^*)^{i-1}_{j,l} \tag{13}$$

It is this effective airfoil that is analyzed by GAUSS2 in order to calculate a pressure distribution.

2.3 Laminar Boundary Layer Solver

The laminar boundary layer solver used is BL3D, which was written by Venkit Iyer (ref. 21). This code is a quick, compressible, three-dimensional solver with fourth-order accuracy in the wall-normal direction. It is applicable to attached laminar flows where the perfect gas and boundary layer assumptions are valid.

Since the solver is being used for two-dimensional applications, the x- and y-momentum, continuity and energy equations are solved step-wise starting at the stagnation point of the flow. The method is iterated at each station until the desired convergence is obtained. After the solution at each station has converged, the derivative of the velocity in the wall-normal direction at the surface is checked to see if the flow has separated. At

each station, the velocity and temperature profiles, their first and second derivatives, and several boundary layer edge conditions are written out for the stability analysis code. These are the only outputs that are needed from this solver. The inputs required are the Mach number, Reynolds number, and the airfoil with its pressure distribution.

2.4 Stability Analysis Code

The stability analysis code used in this method is the COSAL (Compressible Stability Analysis) code written by Mujeeb Malik (ref. 22). In order to obtain the stability properties of three-dimensional compressible boundary layers, COSAL solves the eigenvalue problem by solving an eighth-order system of differential equations. For a two-dimensional case, the problem reduces to a sixth-order system of equations.

Small disturbance theory was used to obtain the basic equations for the linear stability analysis of parallel-flow compressible boundary layers. A set of five ordinary differential equations result from the compressible Navier-Stokes equations and small disturbance theory. These equations are composed of one first-order continuity equation, three second-order momentum equations, and one second-order energy equation. This system can be reduced to a set of eight first-order ordinary differential equations.

Using a finite difference method, COSAL solves the system of basic equations. In order to do this, the eigenvalues are initially obtained through a global eigenvalue search since there are no guesses available. Then, once a guess is obtained, a quick local eigenvalue search is used to continue solving the equations.

COSAL uses temporal stability theory which assumes that the disturbances grow or decay only with time. As a result, the frequency ω is assumed complex,

$$\omega = w_r + i\omega_i, \tag{14}$$

while the wave numbers ζ and ξ are assumed real. The disturbances are said to grow if $\omega_i > 0$, and decay if $\omega_i < 0$.

With a complex group velocity defined as

$$\vec{V}_g = \left(\frac{\partial \omega}{\partial \zeta}, \frac{\partial \omega}{\partial \xi} \right) \tag{15}$$

an N-factor used for transition prediction is calculated using the relation

$$N = \int_{\sigma_1}^{\sigma_2} \frac{\omega_i}{\left| Re\left(\vec{V}_g \right) \right|} d\sigma \tag{16}$$

where σ represents the arc length along a curve on the surface being analyzed.

COSAL can use four different methods to integrate to find the N-Factor at each x-location. These methods include the envelope method, the fixed wavelength and orientation method, the fixed wavelength and frequency method, and the fixed orientation and frequency method. The method used in the current application of COSAL is the envelope method which requires the real frequency ω_r to be specified, and then maximizes the growth rate ω_i with respect to the wave numbers ζ and ξ.

Inputs to COSAL include the real frequency, an initial wave angle and the boundary layer profile data from the laminar boundary layer solver. In this application, the most important output from COSAL is the N-Factor distribution.

When obtaining the stability characteristics of an airfoil, usually a minimum of 10 frequencies must be analyzed by COSAL. For supercritical cases, perhaps as many as 20 or 25 frequencies must be analyzed. At 200 CPU seconds per frequency, COSAL requires at least 2000 CPU seconds, but perhaps as many as 5000 CPU seconds, for each airfoil design iteration. This makes the use of COSAL the most expensive aspect of the method.

Approximately 70% of the time required to use this NLF airfoil design method is spent in COSAL.

2.4.1 Calculation of Analysis N-Factor Distribution

As mentioned above, the envelope method in COSAL is used to obtain the N-Factor distribution of the particular pressure distribution being analyzed. This method requires the real part of the frequency ω_r and an initial wave angle ψ to be specified in order to obtain a unique N-Factor distribution by maximizing the growth rate ω_i with respect to the wave numbers ζ and ξ. An infinite number of frequencies ω_r occur in nature in the flow over an airfoil. Therefore, in theory, in order to calculate the exact N-Factor distribution for the pressure distribution being analyzed, COSAL would have to be used to calculate an N-Factor distribution for every frequency that exists in nature.

Since this is not realistic, the pressure distribution is analyzed for a range of frequencies for each airfoil station j from the stagnation point ($j = 1$) to the laminar separation point ($j = k$). The lower and upper frequencies of this range, denoted by $\omega_{r,min}$ and $\omega_{r,max}$ respectively, and n_f, the number of frequencies to be analyzed within this range, are specified. From n_f, the differential frequency $\Delta\omega_r$ is calculated as

$$\Delta\omega_r = \frac{\omega_{r,max} - \omega_{r,min}}{n_f - 1} \tag{17}$$

This means that the initial frequencies that COSAL will analyze are $\omega_{r,min}$, $\omega_{r,min} + \Delta\omega_r$, $\omega_{r,min} + 2\Delta\omega_r$, ..., $\omega_{r,max} - \Delta\omega_r$, and $\omega_{r,max}$.

The N-Factor at a particular x-location on the airfoil will differ with frequency. For a constant wave angle, the N-Factor at the x-location will increase as the frequency is

increased. However, at some critical frequency $\omega_{r,crit}$, the N-Factor will be a maximum and, as the frequency is increased beyond that, it will start to decrease. This is demonstrated in Figure 2 in which a typical N-Factor is shown over a range of frequencies at a point on an airfoil at a constant wave angle. In general, $\omega_{r,crit}$ is different for each x-location on the airfoil. As a result, even though each of the frequencies in the specified range have been analyzed by COSAL, this does not guarantee that $\omega_{r,crit}$ for each x-location has been determined.

Therefore, a method had to be developed that would ensure that $\omega_{r,crit}$ for each airfoil station was obtained. A flowchart of this method appears as Figure 3. The process begins by defining two variables: N_j and ω_j. With j denoting the airfoil station, N_j is the array of maximum N-Factors, while ω_j is the array of critical frequencies corresponding to the N-Factors of N_j. Initially, both arrays N_j and ω_j are set equal to zero at every j.

When COSAL is called for the first time, the pressure distribution is analyzed at a frequency of $\omega_{r,min}$ and the wave angle ψ. The N-Factor of $\omega_{r,min}$ at station j (defined as $N_{\omega,j}$) is compared to N_j at j. If $N_{\omega,j} > N_j$, then N_j is replaced with the value of $N_{\omega,j}$, and ω_j is replaced with $\omega_{r,min}$. Then, the same process is repeated for each of the frequencies in the frequency range, as shown in the flowchart. After this has been done, N_j contains the first estimate for the array of maximum N-Factors, and ω_j contains the first estimate for the critical frequencies.

However, if any frequency in array ω_j is equal to $\omega_{r,min}$, then the N-Factor at that station j (found in array N_j) is not really the maximum. Using the data in Figure 2 as an example, if the specified frequency range was 30000 Hz to 40000 Hz, then the frequency found in ω_j for this particular station j would be 30000 Hz since the N-Factor at this station is the largest N-Factor in this range. But looking at the figure, the N-Factor at 30000 Hz is not really the maximum. As a result, frequencies below $\omega_{r,min}$ must be analyzed in order to reach the maximum N-Factor for station j. This is accomplished by extending the frequency range by changing the value of $\omega_{r,min}$ to $\omega_{r,min} - \Delta\omega_r$. After analyzing this frequency, array ω_j is checked to see if it is equal to $\omega_{r,min} - \Delta\omega_r$ for any j. If it is, then $\omega_{r,min}$ needs to be modified again. If $\omega_{r,min} - \Delta\omega_r$ does not appear in array ω_j, then no smaller frequencies need to be analyzed.

Conversely, if, after analyzing the specified range of frequencies, any frequency in array ω_j is equal to $\omega_{r,max}$, then a frequency larger than $\omega_{r,max}$ must be analyzed in order to find the maximum N-Factor at that j. This can also be demonstrated by Figure 2. If the specified frequency range was 6000 Hz to 10000 Hz, then 10000 Hz would correspond to $\omega_{r,max}$. Although the N-Factor at 10000 Hz is the largest in this range, it is not the maximum N-Factor for this station. Larger frequencies must be analyzed. After analyzing frequency $\omega_{r,max} + \Delta\omega_r$, array ω_j is checked to see if $\omega_{r,max} + \Delta\omega_r$ appears at any j. If it does, then even a higher frequency must be analyzed. If it doesn't, then N_j is the final array of maximum N-Factors. These N-Factors form the analysis N-Factor envelope or distribution for this particular airfoil at the flow conditions.

2.4.2 Use of N-Factors to Estimate the Transition Location

Since COSAL uses the e^N method, the N-Factors that are calculated can be used to obtain an estimate of the transition location. When the N-Factors exceed a certain value, N_{tr}, transition is estimated to occur at that point.

A wide range of estimates for the value of N_{tr} have been made, depending on whether the correlation was determined from a wind tunnel experiment or an in-flight experiment. Using wind tunnel experiments, values between nine and 11 have been predicted for N_{tr} (refs. 23-24), although values as high as 13.5 have been estimated using in-flight experiments (refs. 10, 25).

2.5 Airfoil Design Method

The airfoil design method used is the CDISC (Constrained Direct Iterative Surface Curvature) method of Richard Campbell (ref. 26). Before designing a new airfoil, the method first modifies the initial target pressures to meet the desired aerodynamic and geometric constraints. Upon obtaining a final target pressure distribution, the method modifies the original airfoil to design a new airfoil that has a pressure distribution closer to the target pressures.

For local Mach numbers less than 1.1, the airfoil is modified to meet the target pressures based on the relation (ref. 26)

$$\Delta C = \Delta C_p \tau \left(1 + C^2 \right)^{0.5} \tag{18}$$

where C is the curvature of the airfoil, ΔC_p is the difference between the target and analysis pressures, and τ is a parameter equal to 1 for the upper surface and -1 for the lower surface. For local Mach numbers greater than 1.1, the relation (ref. 26)

$$\Delta C = \frac{d(\Delta C_p)}{dx}\left(\frac{\tau}{2}\sqrt{M_\infty^2 - 1}\right)\left(1 + \left(\frac{dy}{dx}\right)^2\right)^{-1.5} \tag{19}$$

is initially used, where M_∞ is the free-stream Mach number. As the analysis pressures approach the target pressures, Equation 18 is used with Equation 19 to converge the pressures more quickly.

In addition to using Equations 18 and 19 to modify the airfoil, the angle of attack is adjusted based on the difference between the analysis and target pressures in the leading-edge region.

Some of the parameters constrained in this airfoil design method are the lift and pitching moment coefficients, the maximum airfoil thickness, front and rear spar thicknesses, the leading-edge radius, and the trailing-edge angle.

In this application of the method, the target pressures are modified to meet the aerodynamic constraints prior to using CDISC. Therefore, the target pressures are modified by CDISC only to meet the geometric constraints, not the aerodynamic constraints. Furthermore, the airfoil design method has been modified so that only the lower surface target pressures are changed to meet the geometric constraints. This has been done in an effort not to disturb the amount of NLF that has been achieved on the upper surface.

3.0 Obtaining the Target Pressure Distribution

This chapter is devoted to the discussion of the Target Pressure Design module shown in the flowchart in Figure 1. This module uses the analysis N-Factor distribution from the stability analysis code to calculate a target N-Factor distribution that forces the boundary layer to transition at the desired location. Then, using the analysis and target N-Factors, as well as the analysis pressures, a new target pressure distribution is calculated that is closer to meeting the desired NLF constraints. A new airfoil can then be designed using these target pressures.

The components of the Target Pressure Design module are shown in the flowchart in Figure 4. Each of these components will now be discussed.

3.1 The Target N-Factor Distribution

In order to calculate a target pressure distribution, a target N-Factor distribution that has the desired amount of NLF must be determined, as shown in the first module on the flowchart in Figure 4.

A method has been developed for calculating a target N-Factor distribution from the analysis N-Factors and four control points ($x_{cp,1}$, $x_{cp,2}$, $x_{cp,3}$ and $x_{cp,4}$) specified in the streamwise direction. The first control point, $x_{cp,1}$, is positioned at the location where the analysis N-Factors first exceed an N-Factor level $N_{cp,1}$. In order to calculate a realistic target N-Factor distribution, it is desired to retain the current analysis N-Factors as the target N-Factors ahead of $x_{cp,1}$.

To calculate the target N-Factors aft of $x_{cp,1}$, the target N-Factors desired at the second ($N_{cp,2}$), third ($N_{cp,3}$) and fourth ($N_{cp,4}$) control points are specified. The target N-

Factor distribution is calculated by drawing lines through these four points and smoothing the curve using a polynomial fit.

Since the shape of the target N-Factor distribution is dependent upon the speed regime for which the airfoil is being designed, the values for $N_{cp,1}$, $x_{cp,2}$, $N_{cp,2}$, $x_{cp,3}$, $N_{cp,3}$, $x_{cp,4}$ and $N_{cp,4}$ may vary from one design to the next. Typical values for these parameters will now be discussed for subcritical and supercritical cases.

3.1.1 Subcritical Cases

Using a transition N-Factor of 10 and allowing the flow to transition at 60% chord, a typical target N-Factor distribution for a subcritical case is shown in Figure 5. These target N-Factors were obtained from the analysis N-Factors shown in the same figure, the following control points,

$$x_{cp,2} = 0.58$$

$$x_{cp,3} = 0.60$$

$$x_{cp,4} = 0.65$$

and the desired target N-Factors,

$$N_{cp,1} = 3$$

$$N_{cp,2} = 8$$

$$N_{cp,3} = 10$$

$$N_{cp,4} = 15$$

at these control points. Using $N_{cp,1} = 3$ and the analysis N-Factors shown in the figure, the first control point, $x_{cp,1}$, is located at approximately 18% chord.

There are several reasons for choosing a target N-Factor distribution similar to the one shown in this figure. The region of the target N-Factor distribution ahead of $x_{cp,2}$ forms a buffer zone above which the target N-Factors are not allowed to grow so that the boundary layer will remain laminar prior to the desired transition point at slightly off-design conditions. Beyond $x_{cp,2}$, the target N-Factors are allowed to grow rapidly to force transition. In this case, $x_{cp,3}$ denotes the location of desired transition, which is at 60% chord for a transition N-Factor of 10. It is not necessary, however, for any control point to be located exactly at the desired transition point.

The steep N-Factor gradient beyond $x_{cp,2}$ takes into account the idea that the transition N-Factor may not be exactly 10. In reality, the transition N-Factor could be as low as eight or as high as 15. Even if the transition N-Factor were eight, the airfoil in this case would still have NLF to 55% chord. If the transition N-Factor were 15, then the airfoil would have NLF to 65% chord. This indicates that the flow could actually undergo transition anywhere between 55% and 65% chord, an uncertainty in the transition location of 10% chord.

Suppose that a target N-Factor distribution similar to the one in Figure 6 were used for a subcritical airfoil design. If the transition N-Factor is bounded between eight and 15, then the flow could undergo transition anywhere between 35% and 70% chord. As a result, this is a less desirable target N-Factor distribution since the uncertainty in the transition location of the distribution is greater.

There is, however, a limit on how steep the target N-Factor gradient beyond $x_{cp,2}$ can be. If the N-Factor gradient is too great, then the adverse pressure gradient required to

obtain the target N-Factors in that region will cause the laminar boundary layer to separate in that region. Experience has shown that in order to avoid laminar separation the target N-Factors should not be allowed to grow more than 10 N-Factors for every 10% chord.

3.1.2 Supercritical Cases

In supercritical designs, it is much more difficult to find a realistic target N-Factor distribution. The target N-Factor distribution shown in Figure 5 is not realistic for supercritical airfoil designs. Since the large N-Factor gradient aft of $x_{cp,2}$ would cause an adverse pressure gradient in the target pressure distribution, it is likely that a shock may form ahead of $x_{cp,4}$. In the case of a supercritical airfoil design, this is unwanted since $x_{cp,4}$ denotes the desired location of the shock.

Target N-Factor distributions similar to that seen in Figure 6 were initially used in the design of airfoils in this supercritical regime; however, using these target N-Factor distributions resulted in unrealistic target pressure distributions, which caused a shock to form ahead of $x_{cp,4}$. As a result, since the analysis pressures would never converge to the target pressures in the design of an airfoil, the analysis N-Factors would never converge to the target N-Factors.

After running many cases, a target N-Factor distribution similar to the one shown in Figure 7 was found to be a realistic distribution for supercritical cases. This distribution was obtained using the following control points

$$x_{cp,2} = 0.10$$

$$x_{cp,3} = 0.35$$

$$x_{cp,4} = 0.55$$

and

$$N_{cp,1} = -1$$

$$N_{cp,2} = 0$$

$$N_{cp,3} = 7$$

$$N_{cp,4} = 8$$

The location of $x_{cp,1}$ is at 0% chord since $N_{cp,1} = -1$ and the analysis N-Factor at 0% chord is 0. In this figure, the target N-Factors are allowed to grow rapidly from 10% to 35% chord, where the flow can tolerate the mild adverse pressure gradient that is required to obtain this N-Factor distribution. Then, beyond 35% chord the N-Factors are allowed to grow only by a small amount so that a shock will not form ahead of $x_{cp,4}$.

A result of using a target N-Factor distribution similar to the one shown in Figure 7 is that the uncertainty in the transition location can be large. Since a steep N-Factor gradient is not realistic in supercritical designs, an N-Factor distribution that accounts for the uncertainty in the transition N-Factor is not possible since it is difficult to force the N-Factors to grow much higher than eight or nine. As a result, the design philosophy for supercritical cases is to assume a transition N-Factor near eight. In doing this, the boundary layer will remain laminar until the flow encounters a shock at $x_{cp,4}$. An unfortunate result of this idea is that if the transition N-Factor is 13 in reality, then laminar separation will occur at the shock.

Note how there are no large N-Factor gradients in the distribution beyond 35% chord, which would indicate that there should not be any large changes in the pressure gradient

on the resulting airfoil. Thus, the airfoil that results should have a flat, roof-top pressure distribution that is typical of many supercritical airfoils.

3.2 Extrapolation of Analysis N-Factors

The laminar boundary layer solver is valid only for attached, laminar boundary layers, and is terminated once the laminar boundary layer separates. As a result, the boundary layer solver only supplies data to the stability analysis code as long as the flow is attached. This in turn means that the stability analysis code can only calculate N-Factors until the boundary layer separates.

Suppose that the NLF constraint requires that the flow be attached to 60% chord, but the current airfoil's boundary layer separates at 30% chord. This means that the stability analysis code can only calculate N-Factors to 30% chord, although a target N-Factor distribution will be specified to 60% chord. The N-Factor design method requires analysis and target N-Factors at every station ahead of the fourth control point, which is located at 60% chord in this case. This indicates that the analysis N-Factors must be extended through the separated flow so that the N-Factor design method discussed in Section 3.3.1 can be used. As a result, the next module in the flowchart shown in Figure 4 is used for this purpose.

The method that is used to perform the extrapolation depends on whether the flow is subcritical or supercritical. For subcritical cases, this is accomplished by linear extrapolation based on the analysis pressure distribution. With station $j = k$ being the current location of laminar separation and $j = l$ being the location of the fourth control point, the N-Factors between $k + 1$ and l can be calculated as

$$N_j = N_{j-1} + \frac{N_{j-1} - N_{j-2}}{C_{p,a,j-1,u} - C_{p,a,j-2,u}} (C_{p,a,j,u} - C_{p,a,j-1,u}) \tag{20}$$

where N_j denotes the current analysis N-Factor distribution and $C_{p,a,j,u}$ denotes the current analysis pressure distribution. From experience, for stability of the N-Factor design method the N-Factors calculated by Equation 20 are restricted as follows:

$$N_j \leq N_{j-1} + 150\,(x_j - x_{j-1}) \tag{21}$$

$$N_j \geq 0 \tag{22}$$

For supercritical cases, a different approach is taken. In supercritical flows, it is unlikely that the laminar boundary layer will remain attached through the shock. Moreover, a shock wave is a discontinuity in the pressures and would cause difficulties for the N-Factor design method that is used to design a target pressure distribution. Therefore, calculating N-Factors aft of a shock wave, even if the flow remained attached through the shock, is unnecessary. As a result, in the case of supercritical designs, the laminar boundary layer solver is terminated at the station upstream of the shock wave.

In the case where a shock wave exists ahead of the fourth control point, it is necessary to move the shock aft to the desired location, which is at the fourth control point, so that the N-Factor design method can be used. This is done by imposing a flat roof-top pressure distribution between the current shock location and the fourth control point. If the current shock is at station $j = k$ and the new shock is to be located at $j = l$ (the station representing the fourth control point), then the current shock's upstream pressure coefficient is maintained aft to station l. That is, the analysis pressures between $k + 1$ and l are rewritten as

$$C^{i+1}_{p,a,j,u} = C^{i}_{p,a,k,u} \tag{23}$$

where $C^{i+1}_{p,a,j,u}$ are the new analysis pressures and $C^{i}_{p,a,j,u}$ are the original analysis pressures. This is demonstrated in Figure 8.

Also in this case, analysis N-Factors only exist ahead of station k since the laminar boundary layer solver is terminated at k due to the shock wave. This indicates a need to extrapolate the analysis N-Factors aft to station l so that the N-Factor design method can be used to calculate a target pressure distribution. Since the pressure coefficients between $k+1$ and l are the same, the extrapolation scheme described in Equation 20 cannot be used to calculate a new analysis N-Factor distribution. Therefore, it is assumed that the N-Factors grow only with x, and hence can be written as

$$N_j = N_{j-1} + \frac{N_{j-1} - N_{j-2}}{x_{j-1} - x_{j-2}} (x_j - x_{j-1}) \tag{24}$$

between stations $k+1$ and l.

It is possible, however, that the laminar boundary layer will separate before the shock. In this case, prior to using Equation 24, Equations 20-22 must be used between stations $m+1$ and k, where m is the location of laminar separation and k is the location of the shock.

3.3 The Upper Surface Target Pressures

Now that the analysis and target N-Factor distributions are known, a target pressure distribution can be calculated so that the CDISC airfoil design method can be used to design a new airfoil. The first step in this process is to calculate the upper surface target pressure distribution. In order to do this, the upper surface pressures are divided into two important regions, as shown in Figure 9. In the first region, a new N-Factor design method is used to calculate the target pressures based on the difference between the target

and analysis N-Factors. The pressures in the second region are calculated from the recovery pressures of the first airfoil that was analyzed. The specifics of how the pressures are determined in these two regions will now be discussed.

3.3.1 The N-Factor Design Method

The next module on the flowchart of Figure 4 is used to calculate the upper surface target pressures in the region that extends from the stagnation point of the airfoil to the fourth control point. This is the region where the current pressure coefficients are modified to move the current N-Factor distribution towards the target N-Factor distribution that was prescribed earlier. In order to do this, a new method had to be developed.

In order to achieve the desired amount of natural laminar flow, a method was developed that possessed the following properties:

1. If the current N-Factor at a given airfoil station was larger/smaller than the target N-Factor at that station, then the pressure gradient would have to become more favorable/adverse at that station in order to decrease/increase the current N-Factor.
2. The N-Factor at a given point on the airfoil would be changed by modifying only the pressure coefficient at that point. (This local change in pressure coefficient would have an effect on the N-Factors downstream of the current airfoil station, but not the N-Factors upstream since the boundary layer equations are parabolic.)
3. The design method must produce a smooth and continuous pressure distribution between the stagnation point and the fourth control point.

With these ideas in mind, this method, called the N-Factor design method, was developed such that the change in pressure coefficient required at a given airfoil station j would be governed by the linear relation

$$\frac{\Delta C_{p,j,u}}{\Delta x_j} = A\Delta N_j \tag{25}$$

where

$$\Delta C_{p,j,u} = C_{p,T,j,u} - C_{p,a,j,u} \tag{26}$$

$$\Delta x_j = \left| x_j - x_{j-1} \right| \tag{27}$$

$$\Delta N_j = N_{T,j} - N_j \tag{28}$$

In these equations, A is a relaxation factor (typically 0.50), $C_{p,T,j,u}$ are the new upper surface target pressures, $C_{p,a,j,u}$ are the current upper surface analysis pressures, Δx_j is the grid spacing, $N_{T,j}$ are the target N-Factors, and N_j are the current analysis N-Factors.

Note that Equation 25 satisfies condition 1 above in that for a positive ΔN_j, $\Delta C_{p,j,u}$ is also positive, which induces a more adverse pressure gradient at station j. Conversely, for a negative ΔN_j, $\Delta C_{p,j,u}$ is also negative, which produces a more favorable pressure gradient at station j.

Now in order to satisfy condition 2 above, the N-Factors downstream of station j must be corrected for the change in pressure that has been imposed. This is accomplished by assuming that each N-Factor downstream of station j is increased or decreased by as much as the N-Factor at station j was changed. Effectively, then, ΔN_j is added to each N-Factor downstream of j. Condition 3 above requires that the pressure distribution be both

smooth and continuous. In order to maintain a continuous pressure distribution, the change in pressure applied to station j is also applied to each station downstream of j. In doing this, the pressure distribution remains inherently smooth.

Condition 2 indicates that each N-Factor downstream of j must be corrected for the change in pressure coefficient at j. This perspective can be reversed. If the method is designing at station j, all the modifications in pressures and N-Factors upstream must be taken into account at station j. By solving Equation 25 for $C_{p,T,j,u}$ and correcting for upstream effects as mentioned above, the new relation

$$C_{p,T,j,u} = (C_{p,a,j,u} + \Delta C_{p,j-1,u}) + A\Delta x_j (N_{T,j} - (N_j + \Delta N_{j-1})) \tag{29}$$

is obtained. With $j = 1$ corresponding to the stagnation point, this relation is valid from $j = 2$ to $j = l$, the location of the fourth control point. The boundary conditions at the stagnation point are

$$C_{p,T,1,u} = C_{p,a,1,u} = C_{p,stag} \tag{30}$$

$$N_{T,1} = N_1 = 0 \tag{31}$$

Using COSAL as the stability analysis code, Equation 31 is automatically satisfied as long as the target N-Factor at the stagnation point is set equal to zero.

Figure 10 illustrates how the N-Factor design method is used to calculate the new target pressures. The left-most plot in Figure 10 shows sample analysis and target N-Factor distributions. The change in N-Factor, ΔN, that is required at a grid point is calculated as the difference between the target and analysis N-Factors at that point. The ΔC_p that is necessary to make this change in N-Factor is then calculated using Equation 25. Then, as shown in the center plot in Figure 10, the pressure coefficient at the current grid point and

each grid point downstream is changed by ΔC_p. The analysis N-Factors at the current grid point and each one downstream are changed by ΔN to obtain a modified analysis N-Factor distribution. This is illustrated in the right-most plot of Figure 10. These plots demonstrate how the N-Factor design method is used at one grid point. The same approach is used at each of the grid points over which a target N-Factor distribution is specified.

As mentioned above, the parameter A used in Equation 25 is a relaxation factor in the design process. Using COSAL as the stability analysis code, a typical value for A is 0.50. Although it is not recommended for stability purposes that A be increased above 0.70, A may be decreased if more stability is desired. In addition, the value of A does not seem to be affected by flow parameters like Mach number or Reynolds number.

Perhaps some physical significance can be found in the relationship of Equation 25. As the Tollmien-Schlichting waves propagate downstream, their velocity is

$$v_w = c_w + U, \tag{32}$$

where c_w is the phase velocity of the waves and U is the local velocity of the flow. If the flow is being accelerated (i.e., the velocity U is increasing), then the speed of the wave, v_w, is also increasing. As v_w increases, the T-S waves spread out and their amplitudes decrease, which promotes boundary layer stability. On the contrary, if the flow is being decelerated (i.e., the velocity U is decreasing), then the speed of the wave is also decreasing. As v_w decreases, the T-S waves bunch-up and their amplitudes increase, which increases the instability of the boundary layer. This indicates that there is a negative proportional relationship between a change in the amplitude of the T-S waves and a change in

the local flow velocity. Since the N-Factor is merely the logarithmic growth of the amplitude of the T-S waves, then there is also a negative proportional relationship between a change in N-Factor and a change in the local flow velocity.

There is also a negative inverse relationship between a change in the local pressure gradient and a change in the local flow velocity. As a result, there is a direct relationship between a change in the local pressure gradient and a change in N-Factor, as proposed in Equation 25.

3.3.2 The Pressure Recovery Region

The next module on the flowchart of Figure 4 is used to calculate the upper surface target pressures in the recovery region. The pressure recovery region is composed of the pressures between station $j = l$ and the trailing-edge of the airfoil ($j = n$), as shown in Figure 9. These pressures are formed by modifying the recovery pressures of the first airfoil that was analyzed. $C_{p,j,0}$ denotes the upper surface pressure coefficients of the first airfoil that was analyzed, with j denoting the airfoil station. From this pressure recovery, two intermediate pressure distributions are formed and used to determine the final target pressures in the recovery region. Figure 11 shows this process.

The first intermediate recovery pressure distribution is determined by linearly scaling (see Appendix A, page 89) $C_{p,j,0}$, as shown in Figure 11 (a). The target pressure coefficient at $j = l$ was already determined by the N-Factor design method described in the previous section. Therefore, $C_{p,j,0}$ must be linearly scaled so that its pressure coefficient at station l is the same as the pressure coefficient at station l given by the N-Factor design method. As a result, the first intermediate recovery distribution is given by

$$C_{p,j,1} = \frac{C_{p,T,l,u} - C_{p,n,0}}{C_{p,l,0} - C_{p,n,0}} (C_{p,j,0} - C_{p,n,0}) + C_{p,n,0} \tag{33}$$

Equation 33 is valid from $j = l$ to $j = n$.

The second intermediate recovery distribution is obtained by adding a linear loading distribution onto $C_{p,j,0}$, as shown in Figure 11 (b). This loading distribution is added in order to match the design pitching moment coefficient constraint. The process by which this is done will be described in Section 3.4.2. The second intermediate recovery distribution is then given as

$$C_{p,j,2} = C_{p,j,0} + \frac{1 - x_j}{0.30} C_{p,0.7c} \tag{34}$$

where $C_{p,0.7c}$ denotes the magnitude of the loading distribution at 70% chord. This equation is also valid from $j = l$ to $j = n$.

Now, the final target pressures of the recovery region are obtained by taking a weighted average (see Appendix B, page 91) of the first and second intermediate recoveries, as shown in Figure 11 (c). In doing so, the final target pressures are given by

$$C_{p,T,j,u} = \frac{x_n - x_j}{x_n - x_l} C_{p,j,1} + \frac{x_j - x_l}{x_n - x_l} C_{p,j,2} \tag{35}$$

Being valid from $j = l$ to $j = n$, this expression allows $C_{p,T,j,u}$ to retain the value of $C_{p,j,1}$ at $j = l$ and the value of $C_{p,j,2}$ at $j = n$.

The procedure described in this section is only valid for subcritical flows. For cases where there is a shock wave on the upper surface (at $j = l$ by design), the same process is used to determine the pressure recovery region except that everywhere an "l" appears in

the equations, "$l + 1$" should be put in its place. As a result, then, the equations are only valid from $j = l + 1$ to $j = n$ for supercritical cases.

In order to use these equations from $j = l + 1$ to $j = n$, the target pressure coefficient on the downstream side of the shock ($j = l + 1$) must be calculated using the free-stream Mach number M_∞. The relation (ref. 27)

$$C_p = \frac{2}{1.4M_\infty^2}\left(\left(\frac{1 + 0.2M_\infty^{\,2}}{1 + 0.2M^2}\right)^{3.5} - 1\right) \tag{36}$$

is useful in doing this. Solving Equation 36 for M, the Mach number on the upstream side of the shock is calculated by

$$M_1 = \sqrt{5}\left(\frac{1 + 0.2M_\infty^2}{\left(0.70M_\infty^2 C_{p,T,l,u} + 1\right)^{1/3.5}} - 1\right)^{1/2} \tag{37}$$

Using normal shock theory (ref. 27), the Mach number on the downstream side of the shock is then calculated by

$$M_2 = \left(\frac{1 + 0.2M_1^2}{1.4M_1^2 - 0.2}\right)^{1/2} \tag{38}$$

Using Equation 36, the target pressure coefficient on the downstream side of the shock can then be calculated as

$$C_{p,2} = \frac{2}{1.4M_\infty^2}\left(\left(\frac{1 + 0.2M_\infty^{\,2}}{1 + 0.2M_2^2}\right)^{3.5} - 1\right) \tag{39}$$

However, because of curvature of the airfoil, the pressure coefficient calculated by Equation 39 is not totally correct. To account for curvature effects, the target pressure coefficient on the downstream side of the shock is given as

$$C_{p,T,l+1,u} = \frac{1}{2}(C_p{}^* + C_{p,2}) \tag{40}$$

where $C_p{}^*$ is the sonic pressure coefficient. The process previously discussed can now be used to determine the remainder of the target pressures in the recovery region.

3.4 Meeting the Aerodynamic Constraints

Once this preliminary target pressure distribution is determined, the next module on the flowchart of Figure 4 is used to modify the upper surface target pressures to meet the aerodynamic constraints, which are the lift and pitching moment coefficients. A process was developed by which the upper surface target pressures could be modified to meet these constraints, while changing the N-Factor distribution as little as possible so that the NLF would not be disturbed.

To match these constraints, the upper surface target pressure distribution is divided into three segments. Figure 12 shows a typical upper surface target pressure and target N-Factor distribution, with the pressure distribution being divided into the following three regions:

1. *The leading-edge region.* This region extends from the stagnation point ($j = 1$) to the last point where the target N-Factors are zero ($j = m$).

2. *The center region.* This region extends from airfoil station m to the fourth control point ($j = l$).

3. *The pressure recovery region.* This region extends from station l to the trailing-edge ($j = n$).

The methods by which the target pressures are modified to meet these aerodynamic constraints are discussed in the next two sections. A flowchart showing the procedures of the sections appears as Figure 13.

3.4.1 Lift Coefficient

Since the extent of NLF is dependent upon the pressure gradient, a method for modifying the upper surface target pressures to match the lift coefficient was developed that would maintain the current pressure gradient through the region where the N-Factors are increasing most rapidly. The center region is the region where the N-Factors are most important because they are growing fastest. As a result, it is desired to shift each pressure coefficient in this region by the same amount in order to preserve the current pressure gradient. But, if these pressures are shifted, then the pressures in the leading-edge and pressure recovery regions must also be manipulated so that the pressure distribution remains smooth. In the leading-edge region, the pressures are linearly scaled so that they are continuous at $j = m$, the beginning of the center region.

In order to determine how much the current target pressures $C^{i}_{p,T,j,u}$ are to be modified, it is first assumed that the center region is going to be shifted by $\Delta C_{p,c}$. This would cause a change in lift coefficient of

$$\Delta c_{l,c} = \Delta C_{p,c}\left(\frac{s_l - s_m}{s_n}\right) \tag{41}$$

where s_j represents the chordwise distance from the stagnation point ($j = 1$) defined as

$$s_j = \sum_{k=2}^{j} |x_k - x_{k-1}| \tag{42}$$

If the pressures in the center region are shifted by $\Delta C_{p,c}$, then the pressures in the leading-edge and pressure recovery regions must also be changed, as will be discussed momentarily. The change in lift coefficient in the leading-edge and pressure recovery regions may be approximated by a linear loading variation along the corresponding arc length. Therefore,

$$\Delta c_{l,le} = \frac{1}{2}\Delta C_{p,c}\left(\frac{s_m}{s_n}\right) \tag{43}$$

$$\Delta c_{l,pr} = \frac{1}{2}\Delta C_{p,c}\left(\frac{s_n - s_l}{s_n}\right) \tag{44}$$

As a result, the total change in Δc_l for these changes in pressure would be the sum of Equations 41, 43, and 44, which results in

$$\Delta c_l = \Delta C_{p,c}\left(\frac{1}{2}\frac{s_m}{s_n} + \frac{s_l - s_m}{s_n} + \frac{1}{2}\frac{s_n - s_l}{s_n}\right) \tag{45}$$

Simplifying and solving Equation 45 for $\Delta C_{p,c}$, the amount that the target pressures in the center pressure region must be shifted by is

$$\Delta C_{p,c} = \frac{2 s_n \Delta c_l}{s_l - s_m + s_n} \tag{46}$$

For stability reasons, this equation can be rewritten to include a relaxation factor. In addition, the change in lift coefficient that is needed is actually the difference between the design lift coefficient and the lift coefficient of the current target pressures. So, with a relaxation factor λ (typically 50%), Equation 46 becomes

$$\Delta C_{p,c} = \frac{2\lambda s_n (c_{l,des} - c_l)}{s_l - s_m + s_n} \tag{47}$$

Thus, after calculating $\Delta C_{p,c}$, the new target pressures over the upper surface from $j = m$ to $j = l$ become

$$C^{i+1}_{p,T,j,u} = C^{i}_{p,T,j,u} + \Delta C_{p,c} \tag{48}$$

From $j = 1$ to $j = m - 1$, the upper surface target pressures become

$$C^{i+1}_{p,T,j,u} = \frac{C^{i+1}_{p,T,m,u} - C^{i}_{p,T,1,u}}{C^{i}_{p,T,m,u} - C^{i}_{p,T,1,u}}\left(C^{i}_{p,T,j,u} - C^{i}_{p,T,1,u}\right) + C^{i}_{p,T,1,u} \tag{49}$$

The region between $j = l + 1$ and $j = n$ is the pressure recovery region. Therefore, the method originally used to obtain the pressures in the recovery region (described in Section 3.3.2) is again used to obtain $C^{i+1}_{p,T,j,u}$ from $j = l$ to $j = n$.

As shown in Figure 13, this process is then repeated until

$$\left|c_{l,des} - c_l\right| \leq c_{l,tol} \tag{50}$$

where $c_{l,tol}$ is the desired tolerance for the lift coefficient (typically 0.01).

3.4.2 Pitching Moment Coefficient

Once the design lift coefficient has been achieved, a modification to the pressures in the recovery region is made in an attempt to match the design pitching moment coefficient. The method by which the target pressures in the recovery region are determined is described in Section 3.3.2. In that section, a linear loading distribution with magnitude $C_{p,0.7c}$ at 70% chord was included in Equation 34 for the second intermediate pressure recovery. This exists for the sole purpose of achieving the design pitching moment coefficient.

In order to meet the pitching moment constraint, lift is transferred to or from the pressure recovery region by changing the amount of lift in the loading distribution. This is

accomplished by modifying $C_{p,\,0.7c}$ by adding $\Delta C_{p,\,0.7c}$. The change in lift coefficient of the target pressures resulting from adding $\Delta C_{p,\,0.7c}$ to $C_{p,\,0.7c}$ is

$$\Delta c_l = -\frac{1}{2}(1 - x_l)\,\Delta C_{p,\,0.7c} \tag{51}$$

where x_l represents the location of the fourth control point. This change in lift coefficient causes a change in pitching moment coefficient

$$\Delta c_m = -\Delta c_l\left(x_l - 0.25 + \frac{1 - x_l}{3}\right) \tag{52}$$

Using Equation 51, Equation 52 can be simplified to

$$\Delta c_m = \frac{1}{2}(1 - x_l)\left(\frac{2}{3}x_l + \frac{1}{12}\right)\Delta C_{p,\,0.7c} \tag{53}$$

Simplifying and solving for $\Delta C_{p,\,0.7c}$,

$$\Delta C_{p,\,0.7c} = \frac{24\Delta c_m}{(1 - x_l)\,(8x_l + 1)} \tag{54}$$

Since the change in pitching moment required is actually the difference between $c_{m,\,des}$ and c_m, Δc_m can be replaced with $c_{m,\,des} - c_m$. In addition, Equation 54 can be written to include a relaxation factor ς (typically 50%). As a result, the final expression for $\Delta C_{p,\,0.7c}$ is

$$\Delta C_{p,\,0.7c} = \frac{24\varsigma\,(c_{m,\,des} - c_m)}{(1 - x_l)\,(8x_l + 1)} \tag{55}$$

Therefore, the new value of $C_{p,\,0.7c}$ is

$$C_{p,\,0.7c}^{i+1} = C_{p,\,0.7c}^{i} + \Delta C_{p,\,0.7c} \tag{56}$$

where $C^{i}_{p,\,0.7c}$ is the original value. Using this new value of $C_{p,\,0.7c}$, the target pressures in the recovery region can be recalculated using the method of Section 3.3.2.

After changing the pressures in the recovery region to move c_m towards $c_{m,\,des}$, the lift coefficient of the target pressure distribution was changed. As a result, the method of Section 3.4.1 is used to modify the target pressures to once again achieve the design lift coefficient.

This process is repeated until

$$\left|c_{l,\,des} - c_l\right| \le c_{l,\,tol} \tag{57}$$

and

$$\left|c_{m,\,des} - c_m\right| \le c_{m,\,tol} \tag{58}$$

A typical value for $c_{m,\,tol}$ is 0.01.

3.5 Adjusting the Leading-edge Radius

Since the airfoil design method uses a target pressure distribution to design a new airfoil, the leading-edge radius of the redesigned airfoil depends on the shape of both the upper and lower surface target pressure distributions. As a result, many different target pressure distributions can be used to meet the leading-edge radius constraint. However, it is desirable to use a target pressure distribution that has a reasonable amount of NLF on the lower surface, since the N-Factor design method described in Section 3.3.1 is not used to design the lower surface target pressures to obtain NLF.

In order to do this, the pressure distribution shown in Figure 14 is used to increase the leading-edge radius of the airfoil through modifying the leading-edge target pressures of the upper surface. These pressures were the leading-edge pressures of an airfoil that was

redesigned starting from a NACA 64_1-212 airfoil. The redesigned airfoil had a large extent of NLF on the lower surface and these upper surface pressures seemed to be a contributor to this.

To use these leading-edge pressures, this distribution is linearly scaled so that its pressure coefficient at 30% chord is the same as that of the current target pressures. Then, over the first 30% of the chord, a weighted averaging technique is used to calculate the new target pressures using this distribution and the current target pressures. The pressure coefficient at the leading-edge of the distribution shown in Figure 14 is retained as the new target pressure, while the current target pressure coefficient at 30% chord remains unchanged.

After modifying the target pressures through this averaging, the method of Section 3.4 must be used to modify the upper surface target pressures to meet the aerodynamic constraints. This is shown in the next module of the flowchart of Figure 4.

3.6 The Lower Surface Target Pressures

The next module on the flowchart of Figure 4 is used to calculate the lower surface target pressure distribution. Although the N-Factor design method is not applied to design the lower surface since the lower surface target pressures are modified to meet the geometric constraints, it is desired to obtain as much NLF on the lower surface as possible. In order to do this, the upper surface target pressure distribution is linearly scaled and a weighted average is taken in order to obtain the initial lower surface target pressures. The following process is only applied on the first iteration of the method since it has been seen occasionally to cause the target pressure distribution to change too much from one itera-

tion to the next when many constraints have been imposed. Figure 15 demonstrates the process that is about to be discussed.

The intermediate lower surface target pressures are obtained by linearly scaling the upper surface target pressures, as demonstrated in Figure 15 (a). If $C_{p,T,j,u}$ represents the upper surface target pressures, then the intermediate lower surface target pressures are given as

$$C_{p,j,1} = \frac{C_{p,T,1,u} - C_{p,T,k,u} - \Delta C_{p,k} c_{l,des}}{C_{p,T,1,u} - C_{p,T,k,u}} (C_{p,T,j,u} - C_{p,T,1,u}) + C_{p,T,1,u} \qquad (59)$$

where k denotes the airfoil station closest to 50% chord, and $\Delta C_{p,k}$ is used to cause the final target pressure distribution to have a lift coefficient of $c_{l,des}$. Equation 59 is valid from $j = 1$ (the stagnation point) through $j = n$ (the trailing-edge).

For the region on the lower surface forward of the fourth control point on the upper surface, the pressures represented by Equation 59 are used for the target pressures in the recovery region. That is, from $j = 1$ to $j = l$ (the location of the fourth control point), the lower surface target pressures are given by

$$C_{p,T,j,l} = C_{p,j,1} \qquad (60)$$

For the region aft of station l, the final lower surface target pressures are found by taking a weighted average of the intermediate pressures and the analysis pressures of the recovery region of the initial airfoil that was analyzed, which are denoted by $C_{p,j,0}$. This is demonstrated in Figure 15 (b). As a result, from $j = l + 1$ to $j = n_l$, the lower surface target pressures become

$$C_{p,T,j,l} = \frac{s_j - s_l}{s_{n_l} - s_l} C_{p,j,0} + \frac{s_{n_l} - s_j}{s_{n_l} - s_l} C_{p,j,1} \tag{61}$$

Equation 61 allows $C_{p,T,j,l}$ to retain the value of $C_{p,j,1}$ at $j = l$ and the value of $C_{p,j,0}$ at the trailing-edge. The final target pressure distribution is shown in Figure 15 (c).

It should be mentioned here that these lower surface target pressures will be modified to meet the geometric constraints. Therefore, the amount of NLF that is obtained on the lower surface is directly a function of the geometric constraints imposed. Moreover, since the geometric and aerodynamic constraints constantly react to the changes that the other makes to the pressures, the amount of NLF obtained on the lower surface is also dependent upon the aerodynamic and upper surface NLF constraints.

4.0 Modifying Target Pressures to Enforce Constraints

The flowchart of Figure 1 shows a module above the airfoil design method that is labeled Modify Target Pressures to Enforce Constraints. After a target pressure distribution is calculated as described in Chapter 3, these target pressures are modified while a new airfoil is being designed by the airfoil design method. These changes are needed in order to enforce the desired aerodynamic and geometric constraints.

A flowchart of the Modify Target Pressures to Enforce Constraints module is shown in Figure 16. Each of the components in this module will now be discussed.

4.1 Leading-Edge Pressures

The CDISC airfoil design method directly modifies the airfoil to meet the leading-edge radius constraint, without modifying the target pressure distribution as it does to meet other constraints. As a result, the target pressures are modified within the first module of Figure 16 to account for the change that the airfoil design method made to the leading-edge of the airfoil to meet the leading-edge radius constraint.

This module is not used until 10 iterations through the airfoil design method have been completed. This allows the analysis pressures to approach the desired target pressures in the leading-edge region. But, without modifying the target pressures, the analysis pressures would never exactly match the target pressures in this region, while still maintaining the leading-edge radius constraint.

After completing the first 10 iterations, only the lower surface target pressures are modified. This is done by taking a weighted average ahead of 30% chord of the current lower surface analysis pressures and the current lower surface target pressures. As a result, the new lower surface target pressures become

$$C_{p,T,j,l}^{i+1} = \left(1 - \frac{s_j}{s_k}\right) C_{p,a,j,l}^{i} + \frac{s_j}{s_k} C_{p,T,j,l}^{i} \tag{62}$$

where k represents the station nearest to 30% chord.

During the second 10 iterations through the airfoil design method, only the lower surface target pressures are modified. This allows the upper surface analysis pressures to approach the upper surface target pressures, which have been designed to meet the NLF constraints. After these first 20 iterations have been completed, the upper surface analysis pressures should closely resemble the upper surface target pressures. The new upper surface target pressures are then calculated using a weighted average between the current target and analysis pressures. Therefore, the new upper surface target pressures can be calculated as

$$C_{p,T,j,u}^{i+1} = \left(1 - \frac{s_j}{s_k}\right) C_{p,a,j,u}^{i} + \frac{s_j}{s_k} C_{p,T,j,u}^{i} \tag{63}$$

where k once again denotes the station nearest to 30% chord. In doing this, the upper surface target pressures will usually not change much since the airfoil design method has completed 20 iterations.

4.2 Trailing-Edge Pressures

To meet the trailing-edge angle constraint, the airfoil is modified directly, without changing the target pressures. Therefore, in the next module shown in Figure 16, the trailing-edge target pressures also need to be modified to account for the changes that have been made to the airfoil to meet the trailing-edge angle constraint. On the lower surface, the new target pressures are calculated from the current target and analysis pressures using a weighted average aft of 60% chord. On the upper surface, the new target pressures are calculated from the current target and analysis pressures using a weighted averaged tech-

nique aft of the fourth control point, which is at station l. In the form of equations, the new upper and lower surface target pressures become

$$C_{p,T,j,l}^{i+1} = \frac{s_j - s_k}{s_{n_l} - s_k} C_{p,a,j,l}^{i} + \frac{s_{n_l} - s_j}{s_{n_l} - s_k} C_{p,T,j,l}^{i} \tag{64}$$

$$C_{p,T,j,u}^{i+1} = \frac{s_j - s_l}{s_n - s_l} C_{p,a,j,u}^{i} + \frac{s_n - s_j}{s_n - s_l} C_{p,T,j,u}^{i} \tag{65}$$

where k is the station nearest 60% chord on the lower surface, and l is the location of the fourth control point on the upper surface. These modifications are made at the same frequency that the leading-edge target pressures are modified to account for the leading-edge radius constraint.

The next module on the flowchart of Figure 16 is used to modify the target pressures to meet the aerodynamic constraints. This process was discussed in Section 3.4.

4.3 Releasing Constraints

After modifying the target pressures using the methods of the previous two sections, the next module on the flowchart is used to release one or more of the constraints in the event that the design is over-constrained. In order to do this, a constraint priority list was established. It is as follows:

1. Upper surface NLF
2. Section lift coefficient
3. Leading-edge radius
4. Spar thicknesses
5. Maximum airfoil thickness
6. Trailing-edge angle

7. Pitching moment coefficient

The pitching moment coefficient is the least important constraint and would be the first to be released.

Throughout the design process, the target pressures are constantly being modified to meet each of the design constraints. If the design is not over-constrained, the target pressures will move toward a distribution that satisfies all of the constraints. It is possible, however, that the problem is over-constrained and the target pressures do not move toward any single distribution. It is in this case that one or more of the constraints must be released to allow the target pressures to approach a distribution that meets the more important design constraints.

In order to determine if any of the constraints need to be released, the average amount that the target pressures change by from one iteration to the next is calculated. This change is given by the relation

$$\Delta C_{p,\,av} = \left(\sum_{j=1}^{n} \left| C^{i}_{p,\,T,\,j,\,u} - C^{i-1}_{p,\,T,\,j,\,u} \right| + \sum_{j=2}^{n_l} \left| C^{i}_{p,\,T,\,j,\,l} - C^{i-1}_{p,\,T,\,j,\,l} \right| \right) / \left(n + n_l - 1 \right) \qquad (66)$$

where i denotes the current iteration. If, after 30 iterations through the CDISC airfoil design method,

$$\Delta C_{p,\,av} > 0.10\,, \qquad (67)$$

then a constraint must be released. This criterion was established after running many design cases. It was found that when the design was over-constrained, $\Delta C_{p,\,av}$ was consistently near 0.30 or 0.40 since the target pressures were constantly changing. In the cases where the design was not over-constrained and the target pressures approached a single distribution, $\Delta C_{p,\,av}$ was usually 0.001 or smaller.

There are two reasons why a constraint may be released. First, it just may not be possible to maintain all of the constraints within the specified tolerances, which are typically

$$c_{l,\,tol} = 0.01 \tag{68}$$

$$c_{m,\,tol} = 0.01 \tag{69}$$

$$t_{tol} = 0.001 \tag{70}$$

$$r_{le,\,tol} = 0.0001 \tag{71}$$

$$\phi_{te,\,tol} = 0.50 \tag{72}$$

The cases that are most sensitive to this are the incompressible subcritical cases and the supercritical cases. In these cases, even using different target N-Factor distributions can cause various constraints to be released. This is even more likely when the specified target N-Factor distribution is not realistic.

Next, constraints may be released merely because the design constraints imposed on the airfoil may not be realistic. If one wishes to design a 15% thick airfoil for general aviation applications, but also wants the airfoil to be 9% thick at 20% chord and 7% thick at 60% chord, it is very possible that the thickness constraint is not realistic for the specified front and rear spar constraints. In this case, the thickness constraint would be released according to the constraint priority list specified above.

5.0 Results of the NLF Airfoil Design Method

The NLF airfoil design method described in the previous chapters has been used to design many airfoils. Airfoils have been designed for Mach numbers between 0.10 and 0.80, Reynolds numbers between 1 and 20 million, and maximum thicknesses between 10% and 18% chord. Although the majority of these airfoils have been designed for subcritical cases, a few have been designed for supercritical cases where a shock wave exists on the upper surface of the airfoil.

To demonstrate the method, the results of airfoils designed for a glider, commuter and subsonic transport aircraft are presented in the following three sections.

5.1 Airfoil for a Glider

For the first design case, the NACA 64_1-212 airfoil was redesigned at the following flow conditions:

$$M_\infty = 0.10$$

$$Re = 3 \text{ million}$$

These flow conditions are typical of a glider. For these conditions, the pressure distribution of the NACA 64_1-212 airfoil is shown in Figure 17, while the upper and lower N-Factor distributions are shown in Figure 18. With these flow conditions and a transition N-Factor of 13.5, the laminar boundary layer for both surfaces of this airfoil separated instead of undergoing transition. Since laminar separation is not desired in the design of an airfoil, in the process of redesigning this airfoil a target N-Factor distribution was specified that would force boundary layer transition rather than allow the laminar boundary layer to separate.

It is desired that the redesigned airfoil have the following aerodynamic and geometric characteristics:

$$x_{tr,u} = 0.65$$

$$c_l = 0.30$$

$$c_m = -0.060$$

$$t_{max} = 0.150$$

$$t = 0.120 \text{ at } x = 0.20$$

$$t = 0.090 \text{ at } x = 0.70$$

$$r_{le} = 0.0140$$

Using the NLF airfoil design method, the upper surface analysis N-Factor distribution shown in Figure 18 and the target N-Factor distribution shown in Figure 19 were used to calculate the pressure distribution shown in Figure 20. Then, using the airfoil design method, the airfoil shown in Figure 20 was designed to meet the target pressures calculated by the NLF airfoil design method.

The redesigned airfoil is compared with the NACA 64_1-212 airfoil in Figure 21. In addition, some of the characteristics of the NACA 64_1-212 and the redesigned airfoil are compared in Table 1. In the design of this airfoil, the pitching moment and maximum airfoil thickness constraints were released by the process described in Section 4.3. Nevertheless, the design pitching moment coefficient was coincidentally achieved. The fact that the maximum airfoil thickness constraint was released implies that it was probably not a realistic constraint given the desired front and rear spar thickness constraints.

Only five iterations of the method were required to design the new airfoil, which took nearly four hours on a Silicon Graphics Indigo2 workstation with an R4000 processor.

Table 1. A comparison of the design constraints and the characteristics of the NACA 64_1-212 and the redesigned airfoil at $M_\infty = 0.10$, $Re = 3$ million, and $c_l = 0.30$

	NACA 64_1-212	REDESIGN	CONSTRAINTS
α	1.48	0.67	
c_m	-0.034	-0.062	-0.060
c_d	0.0044	0.0032	
$x_{tr,u}$	0.48 (lam. sep.)	0.66	0.65
$x_{tr,l}$	0.53 (lam. sep.)	0.51 (lam. sep.)	
t_{max}	0.120	0.142	0.150
t at x = 0.20	0.104	0.119	0.120
t at x = 0.70	0.067	0.090	0.090
r_{le}	0.0108	0.0140	0.0140

5.2 Airfoil for a Commuter Aircraft

As the next example, the NLF airfoil design method was used to redesign the NACA 1412 airfoil at a subcritical speed, with the flow conditions being

$$M_\infty = 0.60$$

$$Re = 20 \text{ million}$$

These flow conditions are representative of a commuter aircraft.

The new airfoil was to have the following design characteristics:

$$x_{tr,u} = 0.60$$

$$c_l = 0.40$$

$$c_m = -0.080$$

$$t_{max} = 0.120$$

$$t = 0.095 \text{ at } x = 0.20$$

$$t = 0.070 \text{ at } x = 0.70$$

$$r_{le} = 0.0100$$

For these flow conditions, the pressure distribution of the NACA 1412 airfoil at the design lift coefficient is shown in Figure 22. In addition, the upper and lower surface N-Factor distributions for this airfoil at these conditions are shown in Figure 23. In this figure, an N-Factor of 10 is used to determine where transition from laminar to turbulent flow occurs in the boundary layer.

After calculating the target N-Factor distribution shown in Figure 24, the NLF airfoil design method calculated the target pressure distribution shown in Figure 25. Using this pressure distribution, the airfoil shown in Figure 25 was designed by the CDISC airfoil design method. Figure 26 shows a comparison of the NACA 1412 airfoil and the redesigned airfoil.

Table 2. A comparison of the design constraints and the characteristics of the NACA 1412 and the redesigned airfoil at $M_\infty = 0.60$, $Re = 20$ million, and $c_l = 0.40$

	NACA 1412	REDESIGN	CONSTRAINTS
α	1.78	0.87	
c_m	-0.027	-0.074	-0.080
c_d	0.0054	0.0030	
$x_{tr,u}$	0.21	0.59	0.60
$x_{tr,l}$	0.30	0.48 (lam. sep.)	
t_{max}	0.120	0.120	0.120
t at x = 0.20	0.115	0.096	0.095
t at x = 0.70	0.073	0.068	0.070
r_{le}	0.0156	0.0100	0.0100

Table 2 contains a comparison of some characteristics of the redesigned airfoil with those of the NACA 1412 airfoil at the design flow conditions and lift coefficient. The design constraints are also shown in this table for comparison. With the design method imposing the tolerances specified in Equations 68-72, the redesigned airfoil meets nearly all of the design constraints within the specified tolerances. Table 2 shows a 24 count reduction in drag due to the extent of NLF that was achieved on both surfaces.

It took only six hours to complete the five iterations of the method that were required to redesign this airfoil. Approximately 20% of this time was associated with the Euler solver and CDISC airfoil design method, while 80% of this time was required by the stability analysis code.

To show that the final airfoil is nearly independent of the starting airfoil, the NASA High Speed NLF-0213 airfoil (ref. 8) was redesigned for the same flow conditions and design constraints as for the redesign of the NACA 1412 airfoil.

The pressure distribution of the NASA High Speed NLF-0213 airfoil at $M_\infty = 0.60$, $Re = 20$ million, and $c_l = 0.40$ is shown in Figure 27. The N-Factor envelopes for this pressure distribution and these flow conditions are shown in Figure 28.

After 13 iterations of the NLF airfoil design method, the NASA High Speed NLF-0213 airfoil was successfully redesigned to meet nearly all of the imposed constraints. The analysis and target N-Factor distributions of the redesigned airfoil are shown in Figure 29, while the pressure distribution of the redesigned airfoil is shown in Figure 30. In Figure 31, the redesigned airfoil is compared with the NASA High Speed NLF-0213 airfoil.

Figure 32 shows a comparison of the pressure distributions on the redesigned NASA High Speed NLF-0213 airfoil and on the redesigned NACA 1412 airfoil. Although they are not exactly the same, the pressure distributions do have similar shapes. The main reason that these pressure distributions are not identical is because the upper surface leading-edge pressures of the starting airfoils were very different.

Table 3 was constructed to show the similarities between the characteristics of the two redesigned airfoils. With the exception of the angle of attack required at the design condition and the pitching moment coefficient, both airfoils appear to have identical characteristics. If the pitching moment tolerance $c_{m,tol}$ specified in Equation 69 had been reduced, perhaps the pitching moment coefficients of the two airfoils would be more similar.

Table 3. A comparison of the design constraints and the characteristics of the NASA High Speed NLF-0213 and the two redesigned airfoils at $M_\infty = 0.60$, $Re = 20$ million, and $c_l = 0.40$

	NLF-0213	NLF-0213 REDESIGN	NACA 1412 REDESIGN	CONSTR.
α	1.03	-0.18	0.87	
c_m	-0.014	-0.081	-0.074	-0.080
c_d	0.0042	0.0030	0.0030	
$x_{tr,u}$	0.30	0.59	0.59	0.60
$x_{tr,l}$	0.69 (lam. sep.)	0.48 (lam. sep.)	0.48 (lam. sep.)	
t_{max}	0.132	0.120	0.120	0.120
t at x = 0.20	0.110	0.096	0.096	0.095
t at x = 0.70	0.092	0.068	0.068	0.070
r_{le}	0.0095	0.0100	0.0100	0.0100

In addition, the final target N-Factor envelopes are different, even though they both force transition to occur near 60% chord (see Figures 24 and 28). This may have also been due to the difference in the leading-edge pressures between the two starting airfoils.

Figure 33 shows a comparison of the two redesigned airfoils. They appear to be very different. This is the case since the airfoil design method maintains the trailing-edge ordinates of the starting airfoil throughout the design process. As a result, to better compare the airfoils, the redesigned NASA High Speed NLF-0213 airfoil was rotated to match the average of the trailing-edge ordinates of the redesigned NACA 1412 airfoil. Figure 34 compares the rotated NASA High Speed NLF-0213 redesigned airfoil with the redesigned NACA 1412 airfoil. In this figure, the similarities between these two airfoils can be more easily seen.

In this plot, it appears that the two airfoils have a different leading-edge radius. The leading-edge radius is calculated by fitting a polynomial through the five points that comprise the leading-edge, with these five points being ahead of 0.5% chord. In this region, the airfoils match very well, but then become different in the region between 2% and 20% chord.

It should also be mentioned here that a change in α needs to be made to account for rotating the airfoil. To do this, α would have to be increased by $0.80°$, which would increase the α of the redesigned NASA High Speed NLF-0213 airfoil at the design condition from $-0.18°$ to $0.62°$. This better compares with the angle of attack at the design condition of the NACA 1412 redesigned airfoil, which was $0.87°$.

5.3 Airfoil for a Subsonic Transport Aircraft

As a final example, the NASA Supercritical SC(2)-0412 airfoil (ref. 28) was redesigned for the following flow conditions and constraints:

$$M_\infty = 0.76$$

$$Re = 10 \text{ million}$$

$$x_{tr,u} = 0.55$$

$$c_l = 0.50$$

$$c_m = -0.100$$

$$t_{max} = 0.110$$

$$t = 0.100 \text{ at } x = 0.20$$

$$t = 0.065 \text{ at } x = 0.70$$

$$r_{le} = 0.0150$$

A successful supercritical design is much more difficult to achieve than a subcritical design. With supercritical designs, if the specified target N-Factor distribution is not realistic, then it is not possible to design an airfoil that has the desired target pressure distribution, as was discussed in Section 3.1.2. As a result, trying to find a realistic target N-Factor distribution for a specific supercritical case is often a very tedious process. This was the case in this design.

The pressure distribution of the NASA Supercritical SC(2)-0412 airfoil for the given flow conditions and design lift coefficient is shown in Figure 35. A shock is present on the upper surface near 40% chord. The upper and lower surface N-Factor distributions for this pressure distribution are shown in Figure 36. Using a transition N-Factor of eight for

the reasons discussed in Section 3.1.2, laminar separation occurred at the shock on the upper surface, while laminar separation occurred at 50% chord on the lower surface.

Using the NLF airfoil design method, a new airfoil was designed in eight iterations. The upper and lower surface analysis N-Factors are plotted with the upper surface target N-Factors in Figure 37. Using the target N-Factor distribution shown in Figure 37, the pressure distribution shown in Figure 38 was calculated. Notice how the shock has been moved aft to 55% chord, and appears to be much weaker. Using the airfoil design method, the airfoil shown in this figure was then calculated. The redesigned airfoil is compared with the starting airfoil in Figure 39.

Table 4. A comparison of the design constraints and the characteristics of the NASA Supercritical SC(2)-0412 airfoil and the redesigned airfoil at M_∞ = 0.76, Re = 10 million, and c_l = 0.50

	SC(2)-0412	REDESIGN	CONSTRAINTS
α	1.20	0.58	
c_m	-0.075	-0.101	-0.100
c_d (wave)	0.0017	0.0002	
c_d (total)	0.0058	0.0044	
$x_{tr,u}$	0.41 (shock)	0.55 (shock)	0.55
$x_{tr,l}$	0.53 (lam. sep.)	0.32 (lam. sep.)	
t_{max}	0.120	0.107	0.110
t at x = 0.20	0.109	0.100	0.100
t at x = 0.70	0.073	0.065	0.065
r_{le}	0.0222	0.0150	0.0150

A comparison of the characteristics of the NASA Supercritical SC(2)-0412 and the redesigned airfoil are shown in Table 4. With the exception of the maximum thickness

constraint, the final airfoil meets all of the design constraints imposed, even though the pitching moment constraint was released after five iterations.

Since the laminar boundary layer separated at 32% chord on the lower surface of the redesigned airfoil, the viscous drag was not reduced in the design process. Nevertheless, due to the reduction in wave drag, the total drag of the redesigned airfoil was 14 counts less than that of the starting airfoil. Not only is this a result of moving the shock aft while maintaining the same lift coefficient, but it also results from allowing the N-Factors to grow as much as possible without forcing transition until the shock.

The fact that the boundary layer remained attached on the lower surface only to 32% chord is a result of the geometric constraints that were imposed on the airfoil. As was mentioned previously, the lower surface target pressures are modified to meet the geometric constraints. As a result, if the front spar thickness had been reduced to 9 or 9.5%, then perhaps the airfoil design method would not have had to work so hard to increase the pressures aft of 25% chord in order to meet the maximum thickness constraint. On the other hand, if the front spar thickness had not been reduced, then increasing the desired maximum airfoil thickness to 12% would have given the same effect.

6.0 Concluding Remarks

An automated two-dimensional method has been developed for designing NLF airfoils, while maintaining several other aerodynamic and geometric constraints. The method has been shown to work for a range of Mach numbers, Reynolds numbers, and airfoil thicknesses. The method has also been demonstrated for a supercritical case where a shock wave is present on the upper surface of the airfoil.

In order to develop this NLF airfoil design method, several existing CFD codes were coupled together. In addition, a process was developed for calculating a target N-Factor distribution that forces transition to occur at the desired location. Using this target N-Factor distribution, as well as the current analysis N-Factors and pressures, a method was also developed for calculating a target pressure distribution. Using this target pressure distribution, the current airfoil is redesigned to obtain a new airfoil that is closer to meeting the desired NLF, aerodynamic and geometric constraints. This method has been used to design a number of airfoils, with results shown for glider, commuter and subsonic transport applications.

One advantage of this method is that it is capable of designing an airfoil in a short amount of time. Since an Euler solver has been coupled together with a turbulent boundary layer method to calculate the pressures over the airfoil, the design time is much less than that required for Navier-Stokes codes. As a result, a new airfoil with a large extent of upper surface NLF can be designed in only a few hours.

In addition to the reduction in computer time required, a stability analysis code has been used to calculate N-Factors which are correlated to the transition location. Stability analysis methods have gained respect in the past few years and the prediction of the transition location that results is taken as being fairly accurate. In this method, the stability

analysis code is automated to calculate the N-Factor distribution by varying the frequency of the T-S waves while assuming that the disturbances grow only in time. Since an N-Factor distribution is calculated to determine the transition location of the airfoil, a design philosophy is presented for specifying a target N-Factor distribution for both subcritical and supercritical airfoil designs. Subcritical target N-Factor distributions are specified so that the flow does not undergo transition at slightly off-design conditions and reduces the uncertainty of the transition location by forcing the N-Factors to grow rapidly through the desired transition location. In supercritical designs, a target N-Factor distribution is specified that forces the flow to transition before the shock so that laminar flow is not terminated at the shock.

In order to design a new airfoil that possesses the desired target N-Factor distribution, an N-Factor-Target Pressure relationship was developed. This N-Factor design method relates a change in N-Factor at an x-location to a change in the local pressure gradient. In addition, this method is independent of Mach number and Reynolds number.

Another attribute of the method is that it is capable of maintaining several aerodynamic and geometric constraints. A method was established to meet these constraints while also maintaining the desired amount of NLF on the upper surface of the airfoil. The approach implemented to meet these aerodynamic and geometric constraints is new. The method dictates that the upper surface target pressures are modified to meet only the NLF and aerodynamic constraints while the lower surface target pressures are modified to meet only the geometric constraints.

This method has also been shown to be robust. If enough design constraints are imposed, the airfoil that results is largely independent of the starting airfoil. Another advantage of this method is that the codes used have been coupled together in modular

form. This allows for other codes to be used in the place of any of the current components. The NLF airfoil design method works efficiently and well to design new NLF airfoils. Only by using this method could one appreciate how great it really works.

There are several possibilities for extension of this research. The method could be applied to bodies other than airfoils and wings, with possible applications including fuselages and nacelles. In addition, the method could be extended to the design of airfoils for supersonic applications. Since large sweep angles are needed for supersonic wings, crossflow instabilities would be a major issue. In these cases, boundary layer suction and blowing is often necessary to help reduce the crossflow disturbances. As a result, when extending the method to include supersonic designs, the method may also have to be modified to account for suction and blowing.

7.0 References

1) Jacobs, E.N.: "Preliminary Report on Laminar-Flow Airfoils and New Methods Adopted for Airfoil and Boundary-Layer Investigations," NACA WR L-345, June 1939.

2) Theodorsen, T; and Garrick, I.E.: "General Potential Theory of Arbitrary Wing Sections," NACA Report No. 452, 1933.

3) Abbott, I.H.; and von Doenhoff, A.E.: Theory of Wing Sections, Dover Publications, 1949, pp. 62-63, 118-120.

4) Srokowski, A.J.; and Orszag, S.A.: "Mass Flow Requirements for LFC Wing Design," AIAA 77-1222, August 1977.

5) Kanner, H.S.: "Design of a High Subsonic Supercritical Full-Chord Laminar Flow Airfoil with Boundary Layer Suction at High Design Lift Coefficients," Master's Thesis, George Washington University, 1994.

6) Hanks, G.W.: "Natural Laminar Flow Airfoil Analysis and Trade Studies," NASA CR-159029, May 1979.

7) McGhee, R.J.; Viken, J.K.; Pfenninger, W.; Beasley, W.D.; and Harvey, W.D.: "Experimental Results for a Flapped Natural-Laminar-Flow Airfoil with High/Lift Drag Ratio," NASA TM-85788, May 1984.

8) Sewall, W.G.; McGhee, R.J.; Viken, J.K.; Waggoner, E.G.; Walker, B.S.; and Millard, B.F.: "Wind Tunnel Results for a High-Speed, Natural Laminar-Flow Airfoil Designed for General Aviation Aircraft," NASA TM-87602, November 1985.

9) Somers, D.M.: "Design and Experimental Results for a Natural-Laminar-Flow Airfoil for General Aviation Applications," NASA TP-1861, June 1981.

10) Viken, J.K.: "Aerodynamic Design Considerations and Theoretical Results for a High Reynolds Number Natural Laminar Flow Airfoil," Master's Thesis, George Washington University, 1983.

11) Rozendaal, R.A.: "Variable Sweep Transition Flight Experiment (VSTFE)-Parametric Pressure Distribution Boundary Layer Stability Study and Wing Glove Design Task," NASA CR-3992, June 1986.

12) Dodbele, S.S.: "Design Optimization of Natural Laminar Flow Bodies in Compressible Flow," NASA CR-4478, December 1992.

13) Dodbele, S.S.; van Dam, C.P.; and Vijgen, P.M.H.W.: "Design of Fuselage Shapes for Natural Laminar Flow," NASA CR-3970, March 1986.

14) Dodbele, S.S.; van Dam, C.P.; Vijgen, P.M.H.W.; and Holmes, B.J.: "Shaping of Airplane Fuselages for Minimum Drag," *Journal of Aircraft*, Vol. 24, May 1987, pp. 298-304.

15) Hartwich, P.M.: "Comparison of Coordinate-Invariant and Coordinate-Aligned Upwinding for the Euler Equations," *AIAA Journal*, Vol. 32, No. 9, September 1994, pp. 1791-1799.

16) Hartwich, P.M.: "Euler Study on Porous Transonic Airfoils with a View Toward Multipoint Design," *Journal of Aircraft*, Vol. 30, No. 2, March-April 1993, pp. 184-191.

17) Hartwich, P.M.: "Fresh Look at Floating Shock Fitting," *AIAA Journal*, Vol. 29, No. 7, July 1991, pp. 1084-1091.

18) Stratford, B.S.; and Beavers, G.S.: "The Calculation of the Compressible Turbulent Boundary Layer in an Arbitrary Pressure Gradient - A Correlation of Certain Previous Methods," R. & M. No. 3207, British Aeronaut. Res. Coun., September 1959.

19) Keith, J.S.; Ferguson, D.R.; Merkle, C.L.; Heck, P.H.; and Lahti, D.J.: "Analytical Method for Predicting the Pressure Distribution about a Nacelle at Transonic Speeds," NASA CR-2217, March 1973.

20) Squire, H.B.; and Young, A.D.: "The Calculation of the Profile Drag of Aerofoils," R. & M. No. 1838, British Aeronaut. Res. Coun., 1938.

21) Iyer, V.: "Computation of Three-Dimensional Compressible Boundary Layers to Fourth-Order Accuracy on Wings and Fuselages," NASA CR-4269, January 1990.

22) Malik, M.R.: "COSAL - A Black-Box Compressible Stability Analysis Code for Transition Prediction in Three-Dimensional Boundary Layers," NASA CR-165925, May 1982.

23) Malik, M.R.: "Stability Theory Applications to Laminar-Flow Control," Research in Natural Laminar Flow and Laminar-Flow Control, NASA CR-2487, 1987, pp. 219-244.

24) Viken, J.K.: "Boundary-Layer Stability and Airfoil Design," Laminar Flow Aircraft Certification, NASA CR-2413, 1985, pp. 1-30.

25) Horstmann, K.H.; Quast, A.; and Redeker, G.: "Flight and Windtunnel Investigations on Boundary Layer Transition at Reynolds Numbers up to 10^7," ICAS pare 88-3.7.1, 1988.

26) Campbell, R.L.: "An Approach to Constrained Aerodynamic Design with Application to Airfoils," NASA TP-3260, November 1992.

27) Anderson, J.D.: Modern Compressible Flow: with Historical Perspective, 2nd Edition, McGraw-Hill Publishing Company, 1990, pp. 67, 278.

28) Harris, C.D.: "NASA Supercritical Airfoils - A Matrix of Family-Related Airfoils," NASA TP-2969, March 1990.

29) Mineck, R.E; Campbell, R.L.; and Allison, D.O.: "Application of Two Procedures for Dual-Point Design of Transonic Airfoils," NASA TP-3466, September 1994.

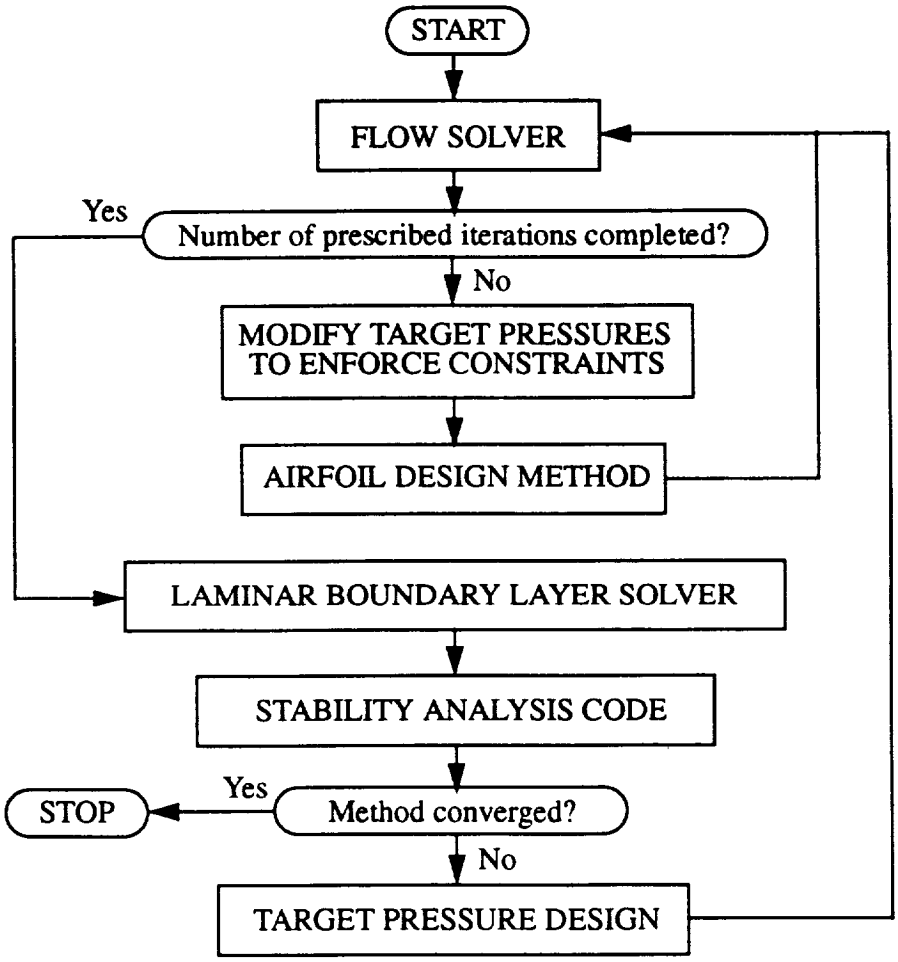

Figure 1. A flowchart of the NLF airfoil design method

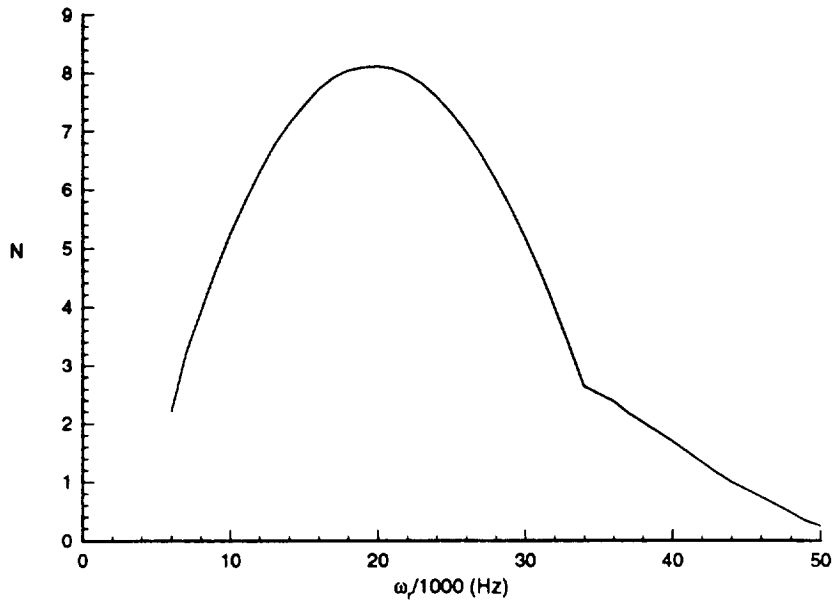

Figure 2. A typical variation of N-Factor (N) with frequency (ω_r) at any x-location on an airfoil for a constant wave angle (ψ)

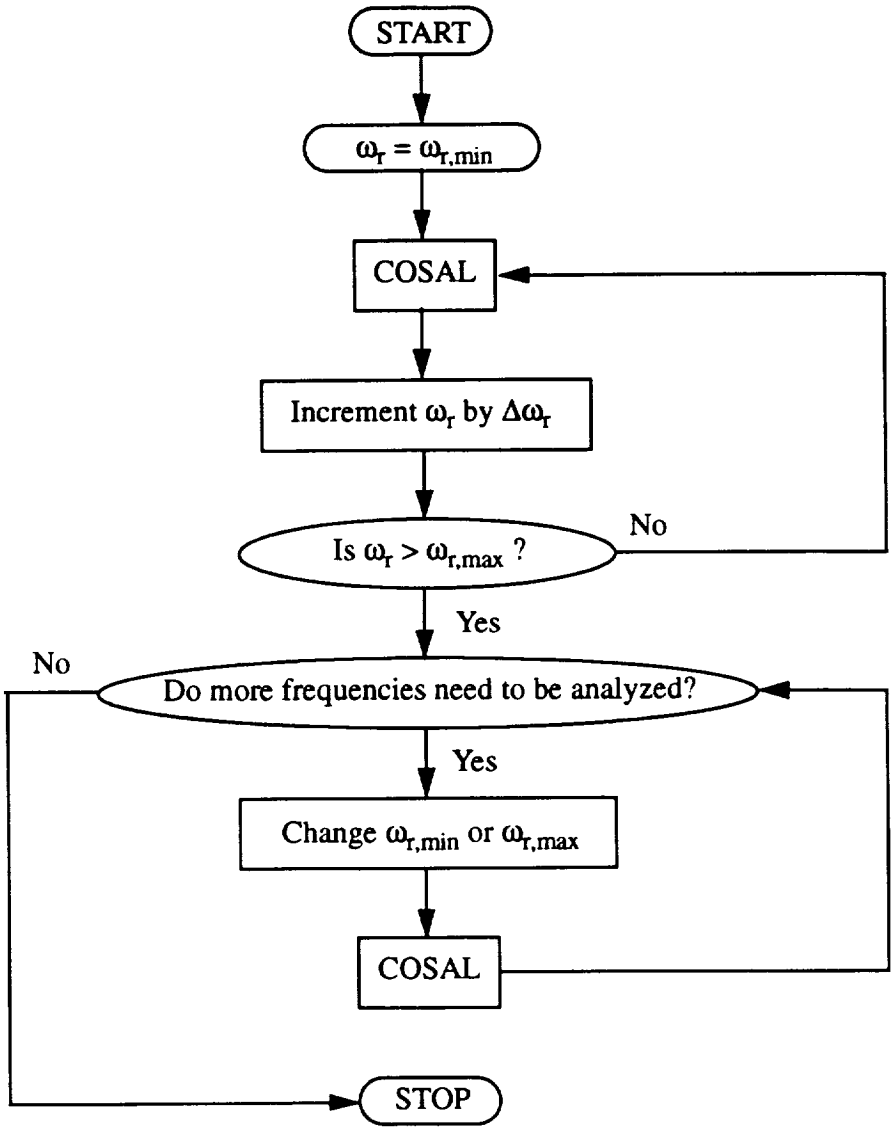

Figure 3. A flowchart of how COSAL is used to calculate the analysis N-Factor distribution for a pressure distribution

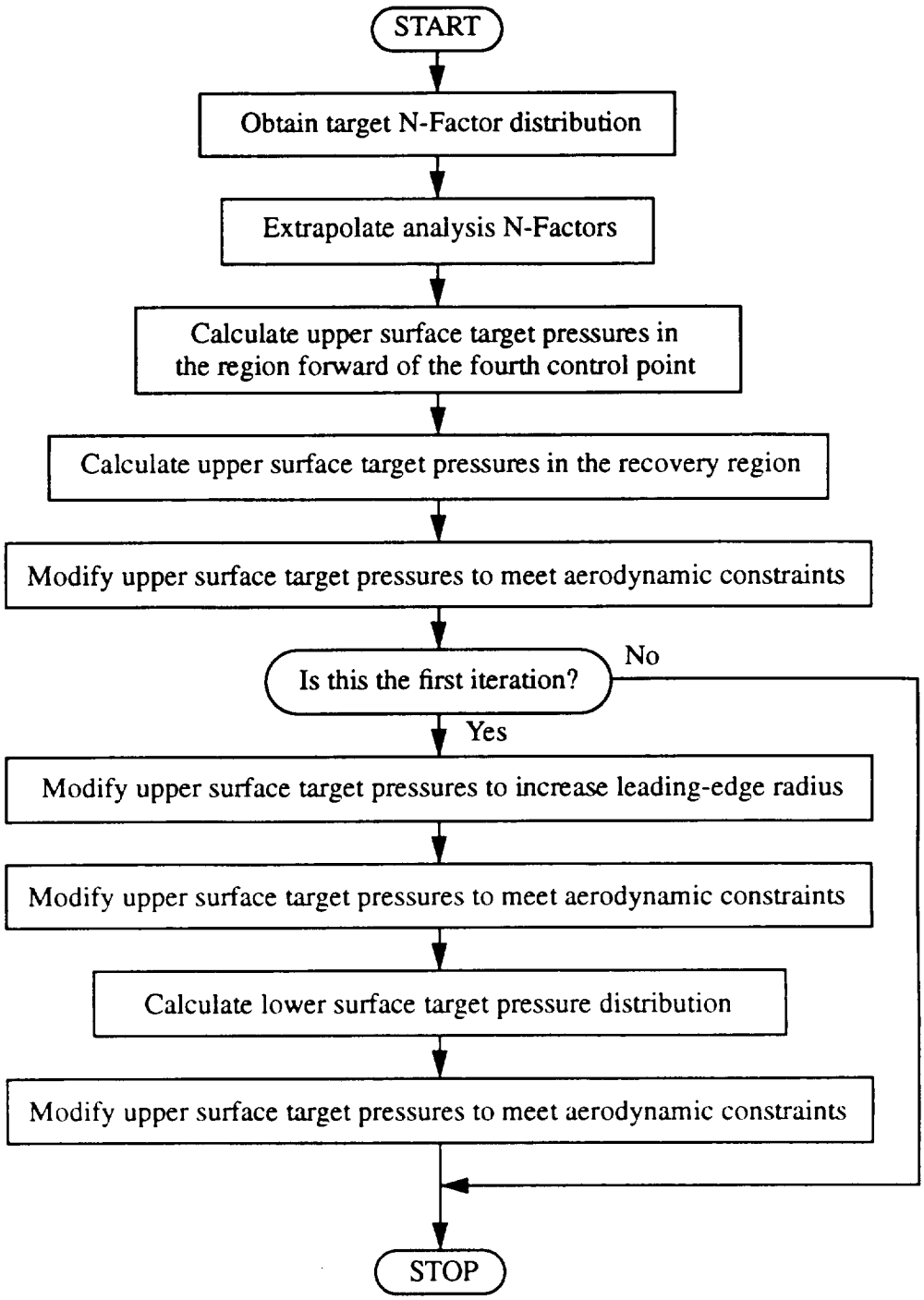

Figure 4. A flowchart of the Target Pressure Design module

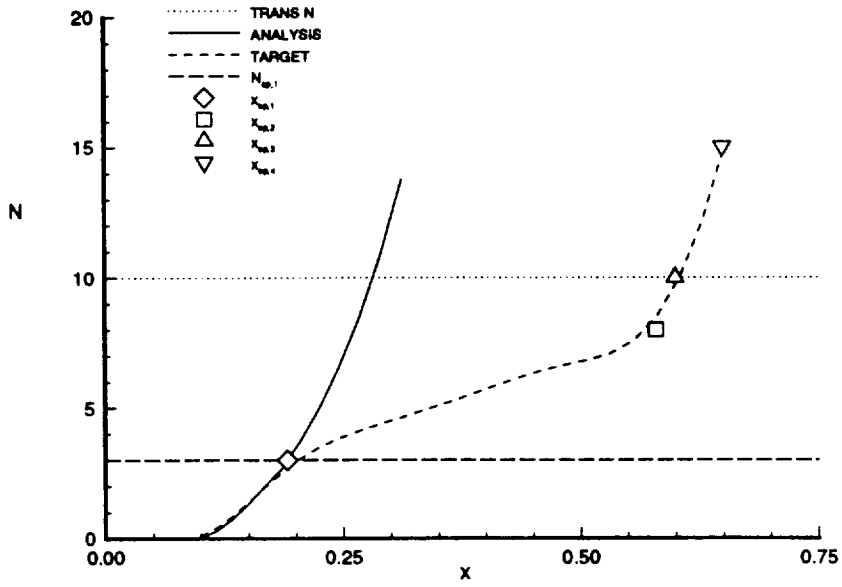

Figure 5. A typical subcritical target N-Factor distribution calculated by the Target Pressure Design module

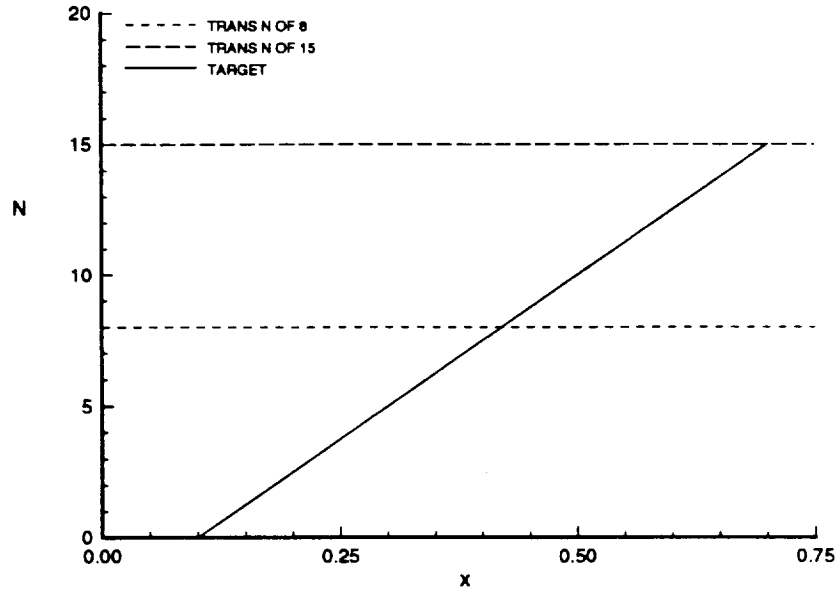

Figure 6. An example of an undesirable target N-Factor distribution for both subcritical and supercritical airfoil designs

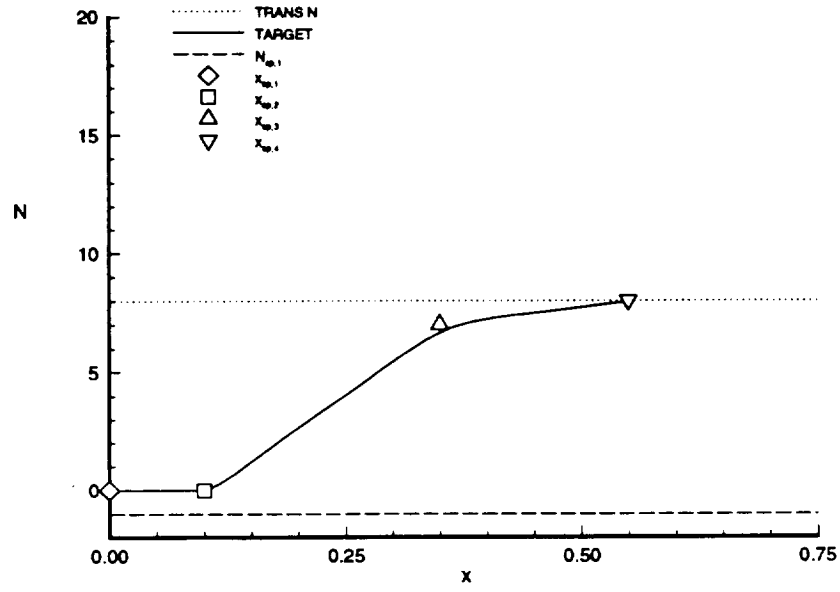

Figure 7. A typical supercritical target N-Factor distribution

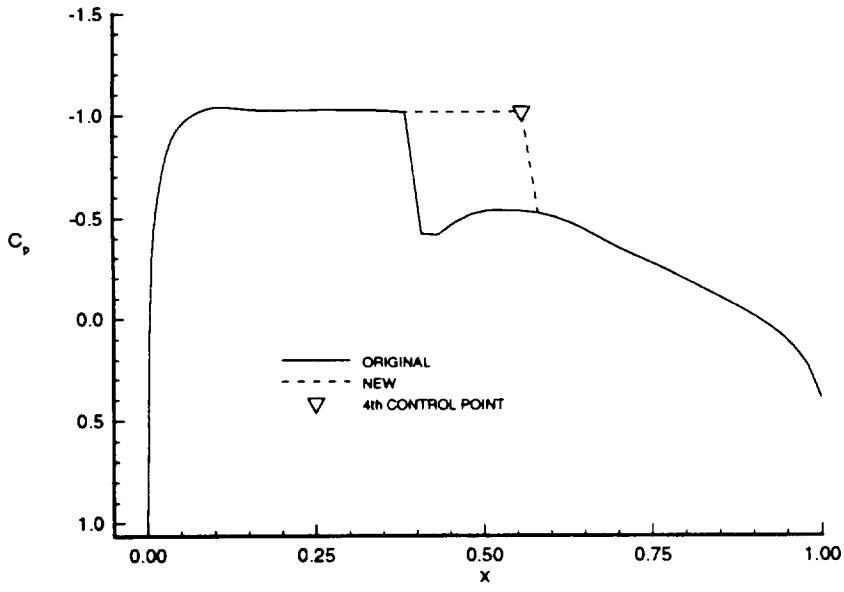

Figure 8. An example of how an upper surface pressure distribution is modified to move a shock back to 55% chord

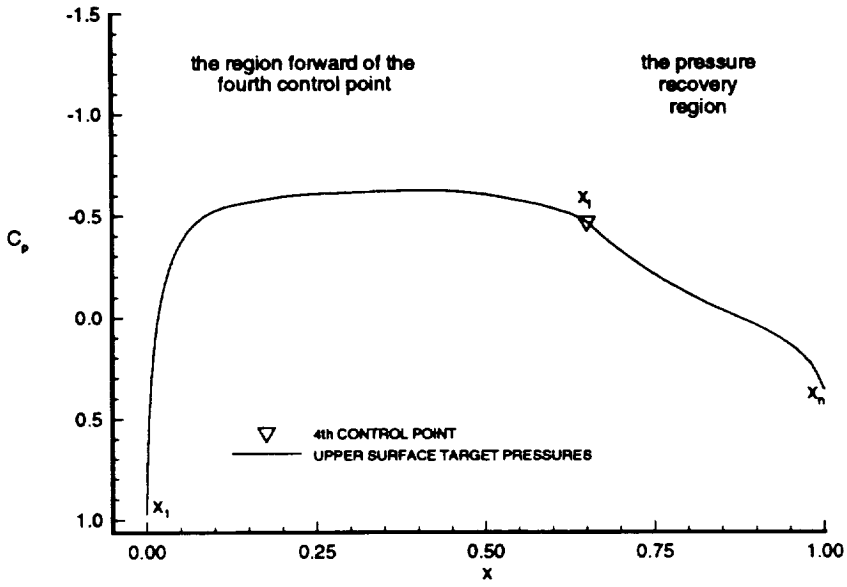

Figure 9. The two regions that the upper surface pressures are divided into to calculate the target pressure distribution

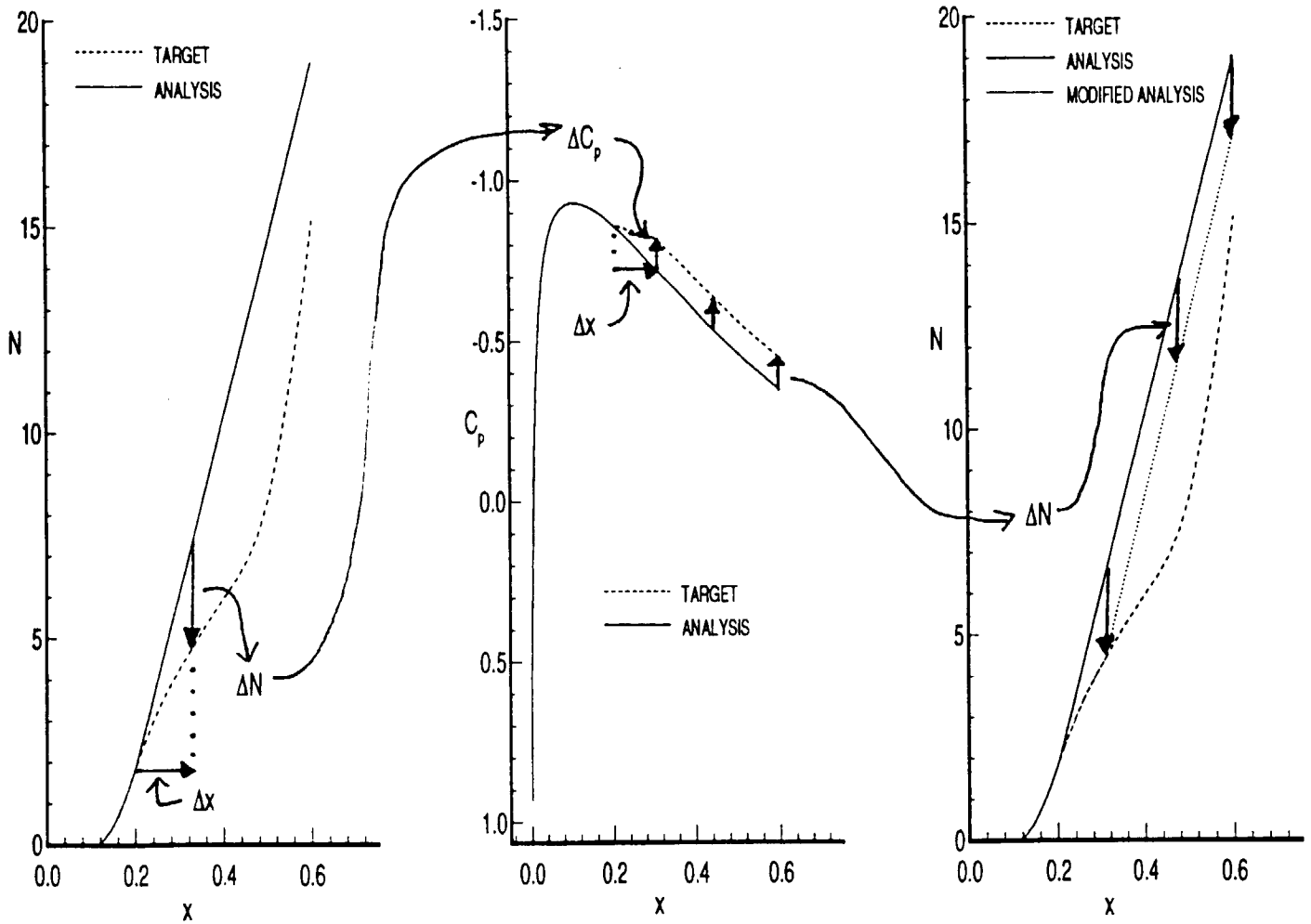

Figure 10. An illustration of how the N-Factor design method is used to calculate the new target pressures

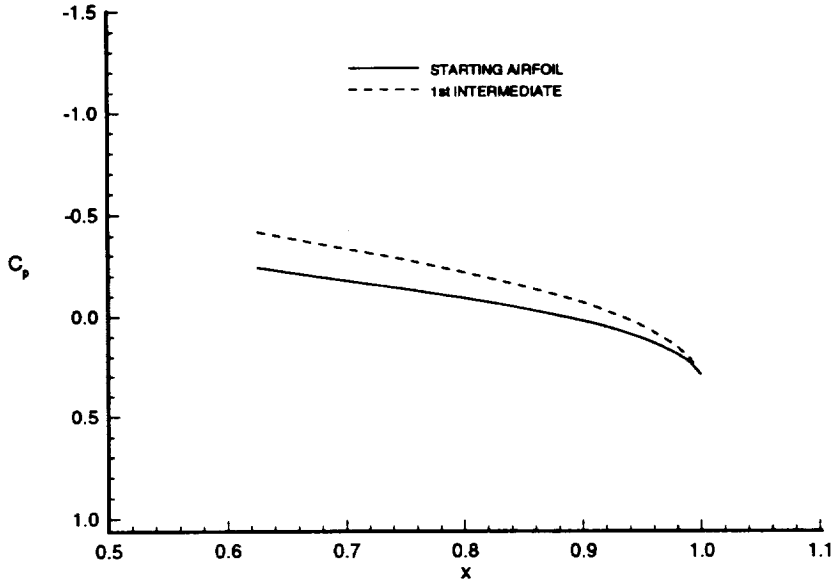

(a) The first intermediate recovery pressures

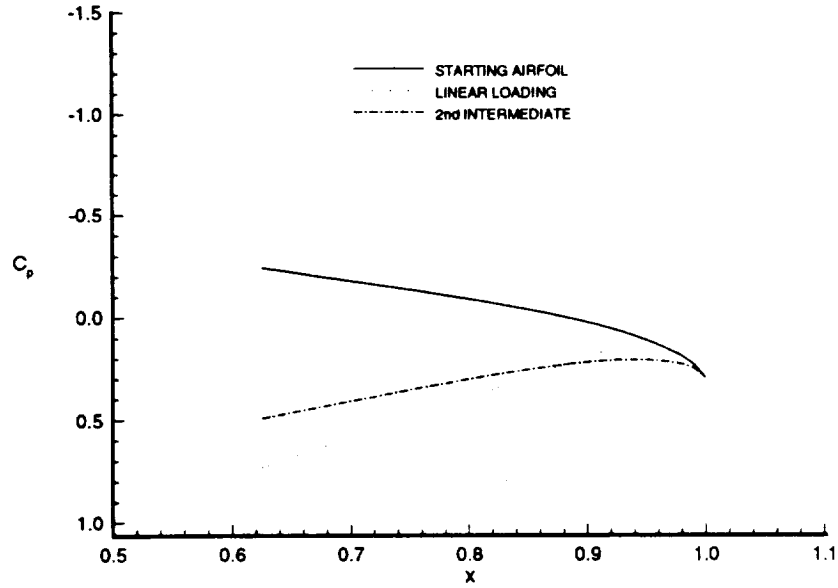

(b) The second intermediate recovery pressures

Figure 11. The evolution of the target pressures in the recovery region

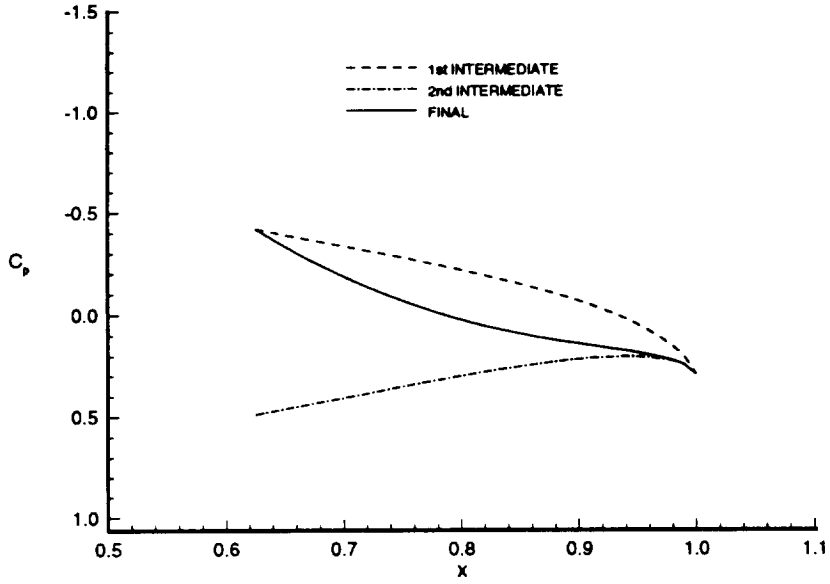

(c) The final target pressures in the recovery region

Figure 11. Concluded

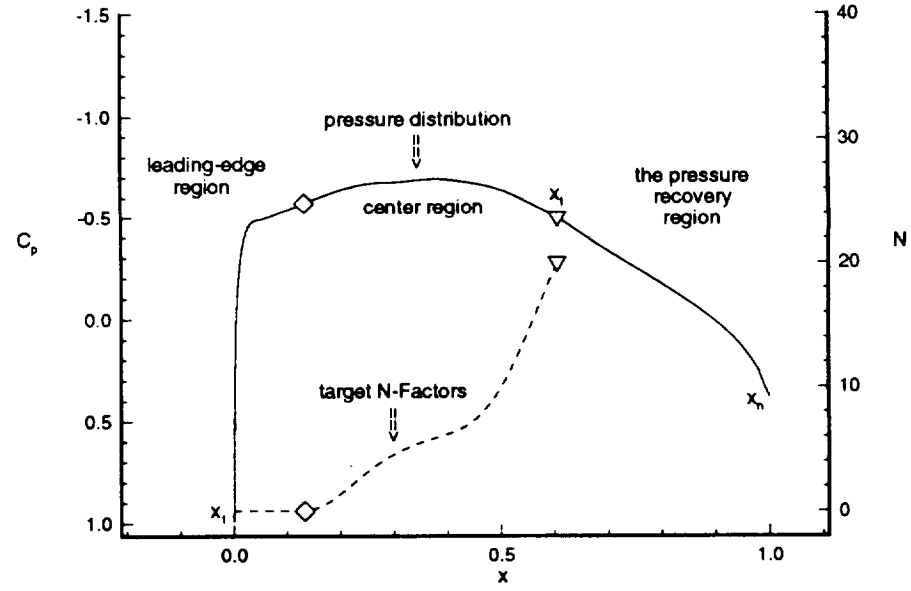

Figure 12. The three regions that the upper surface target pressures are divided into in order to obtain the lift and pitching moment coefficients

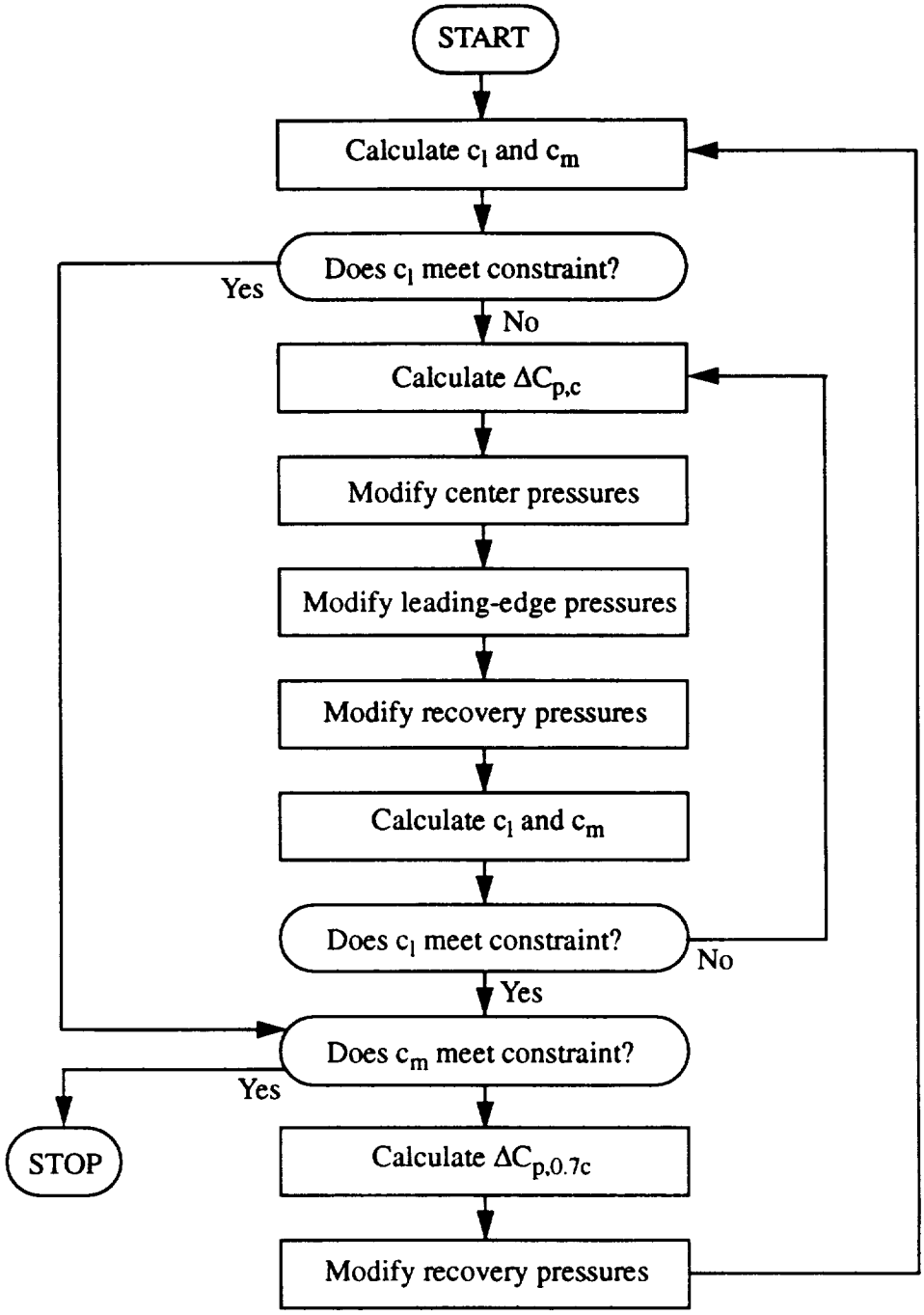

Figure 13. A flowchart of the method by which the target pressures are modified to meet the aerodynamic constraints

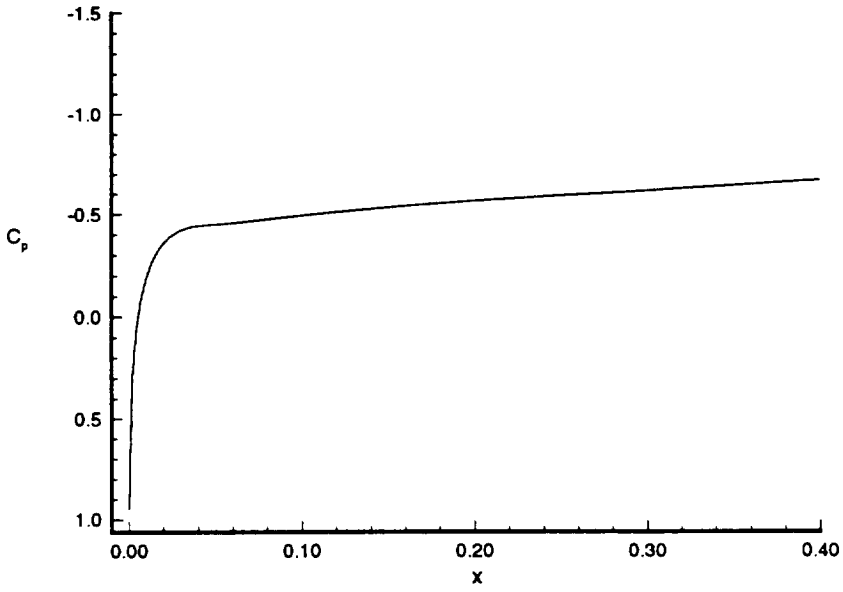

Figure 14. The upper surface pressure distribution that is used to increase the leading-edge radius of the airfoil

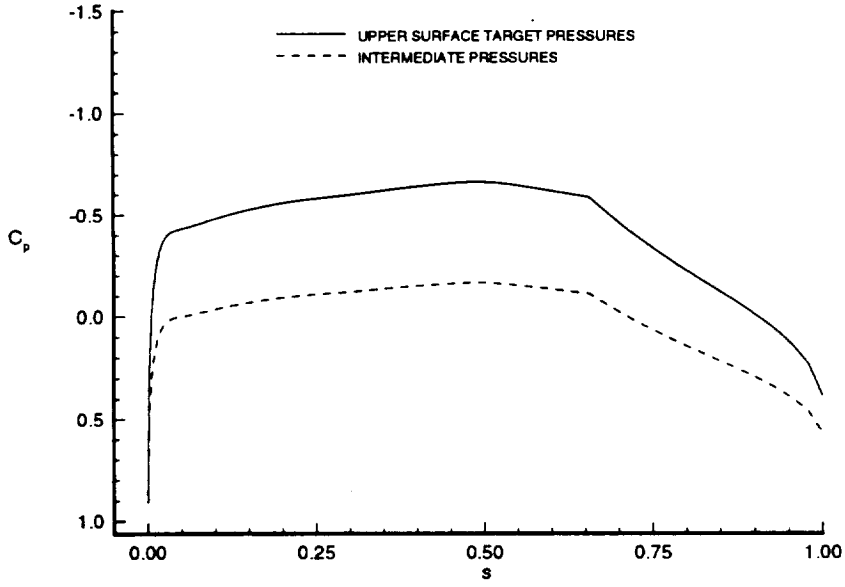

(a) Linearly scaling the upper surface target pressures

Figure 15. The evolution of an initial lower surface target pressure distribution

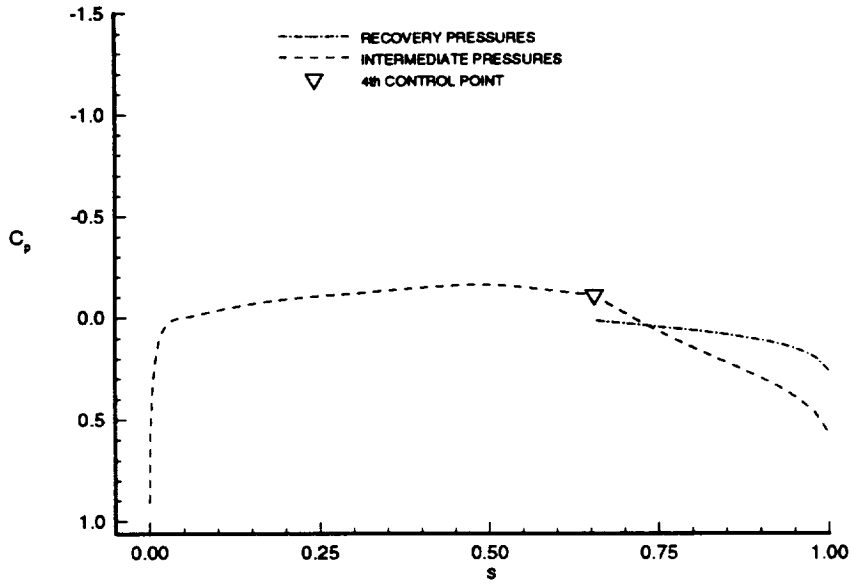

(b) The lower surface recovery pressures

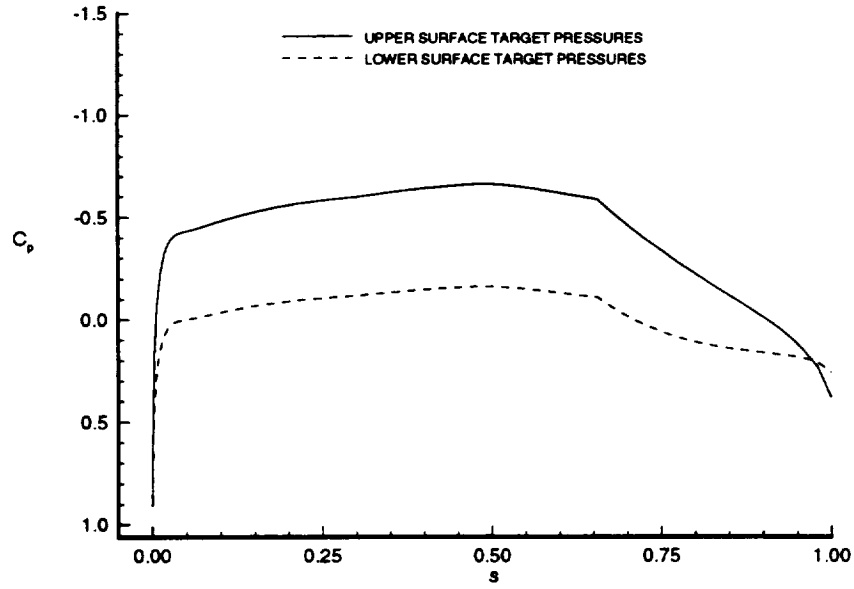

(c) The initial target pressure distribution

Figure 15. Concluded

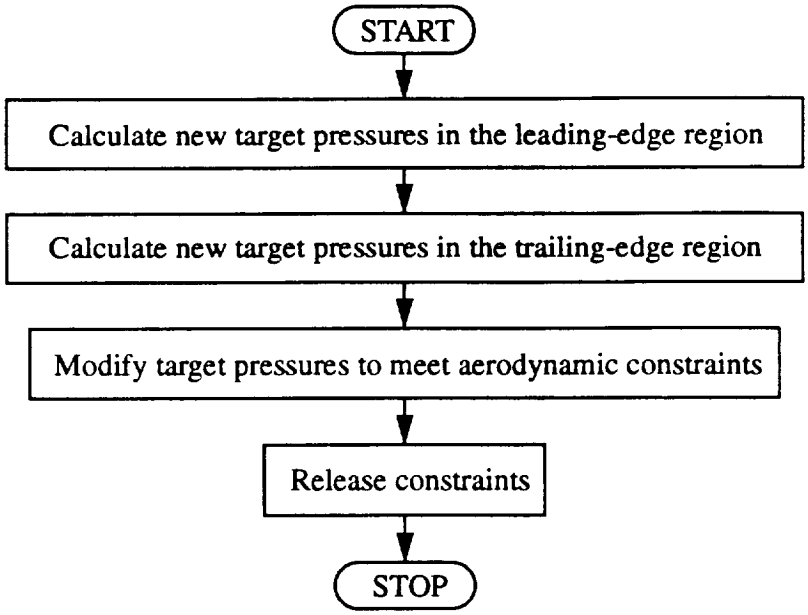

Figure 16. A flowchart of the module for Modifying Target Pressures to Enforce Constraints

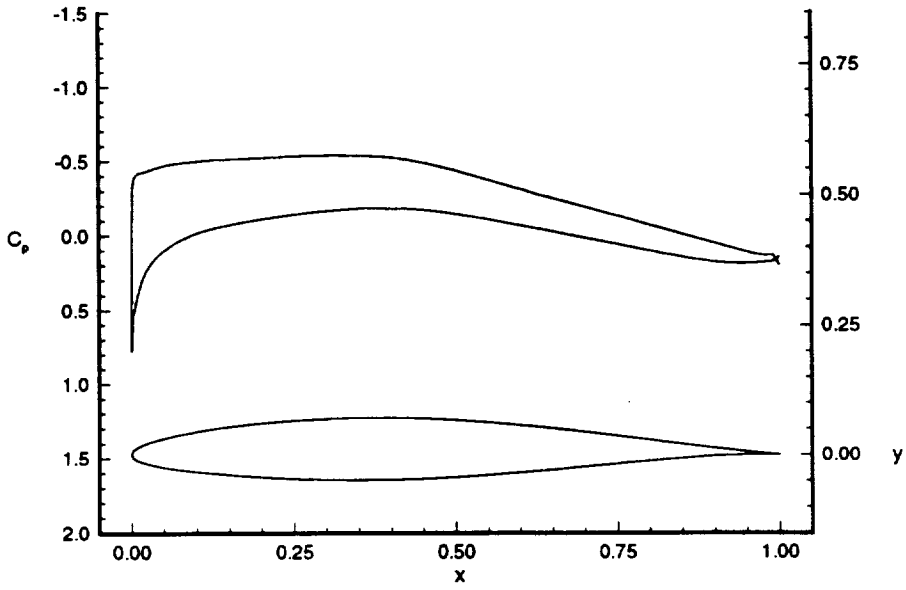

Figure 17. The pressure distribution and shape of the NACA 64_1-212 airfoil at $M_\infty = 0.10$, $Re = 3$ million, and $c_l = 0.30$

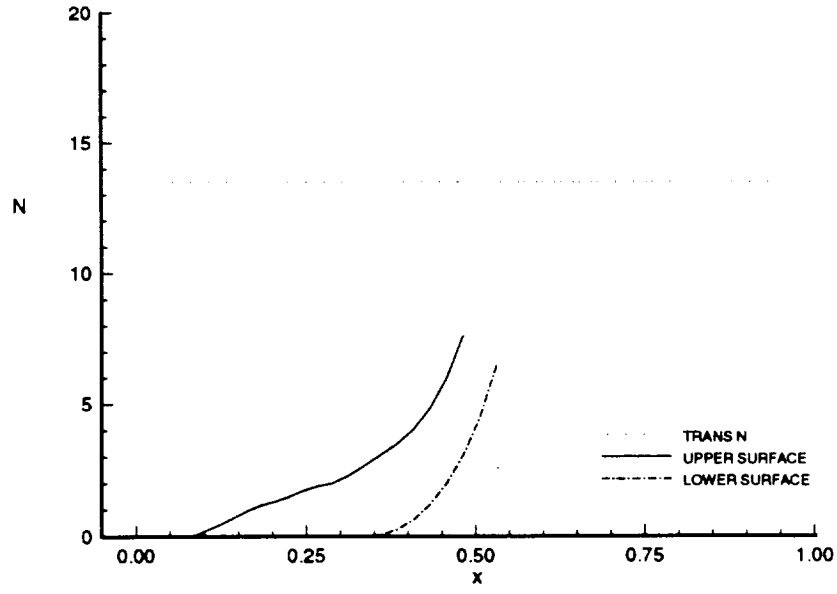

Figure 18. The upper and lower surface N-Factor distributions of the NACA 64_1-212 airfoil at $M_\infty = 0.10$, $Re = 3$ million, and $c_l = 0.30$

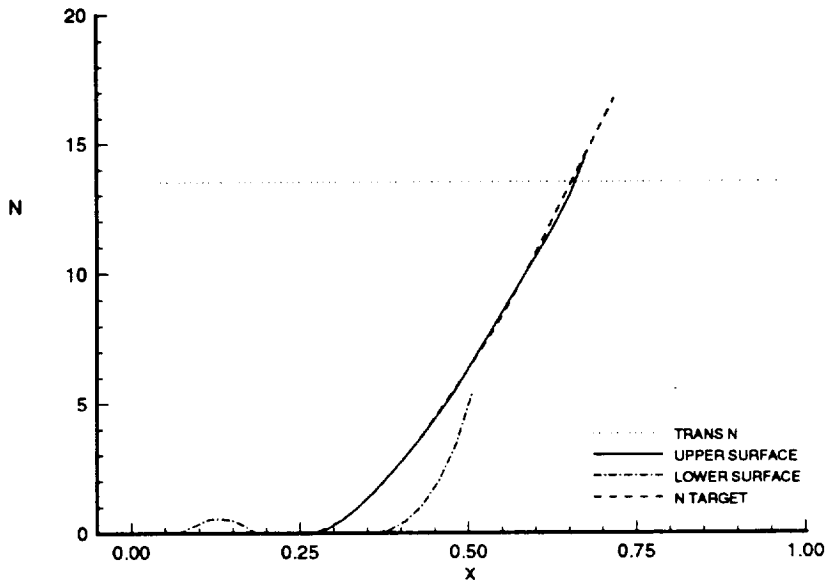

Figure 19. The upper and lower surface N-Factor distributions of the redesigned NACA 64_1-212 airfoil at $M_\infty = 0.10$, $Re = 3$ million, and $c_l = 0.30$

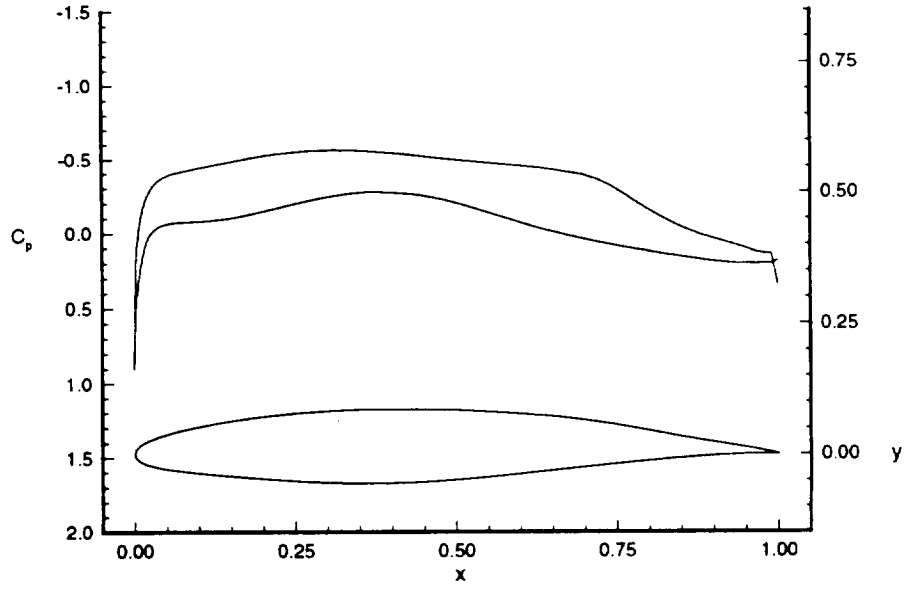

Figure 20. The pressure distribution and shape of the redesigned NACA 64_1-212 airfoil at $M_\infty = 0.10$, $Re = 3$ million, and $c_l = 0.30$

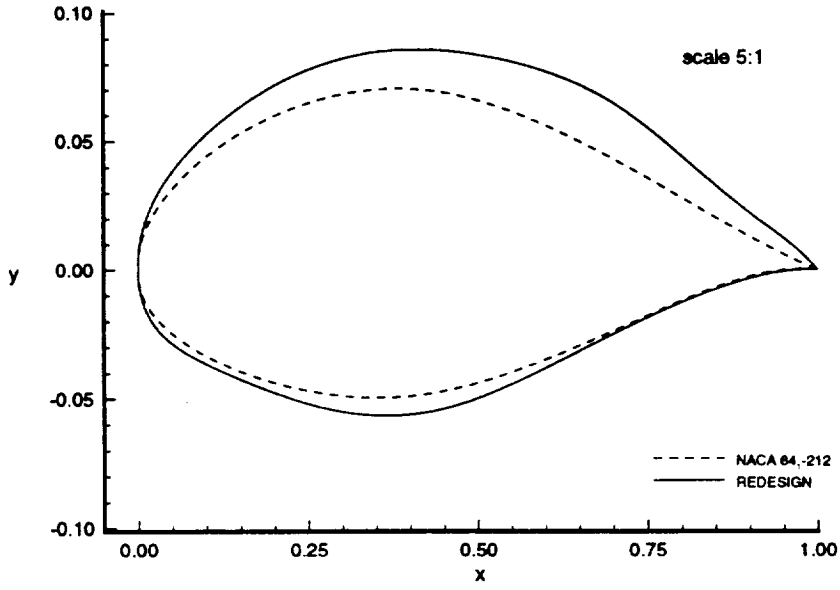

Figure 21. A comparison of the NACA 64_1-212 airfoil and the redesigned NACA 64_1-212 airfoil

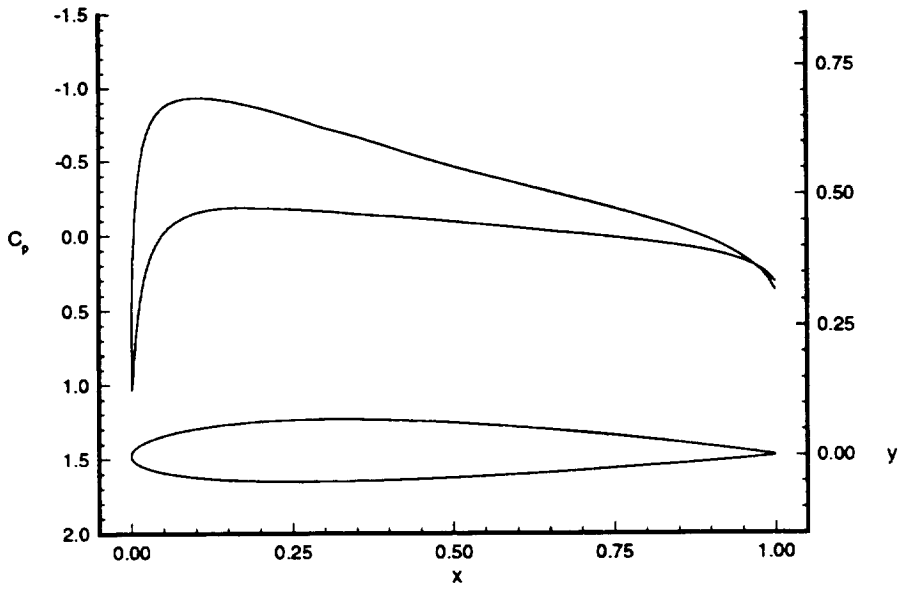

Figure 22. The pressure distribution and shape of the NACA 1412 airfoil at $M_\infty = 0.60$, $Re = 20$ million, and $c_l = 0.40$

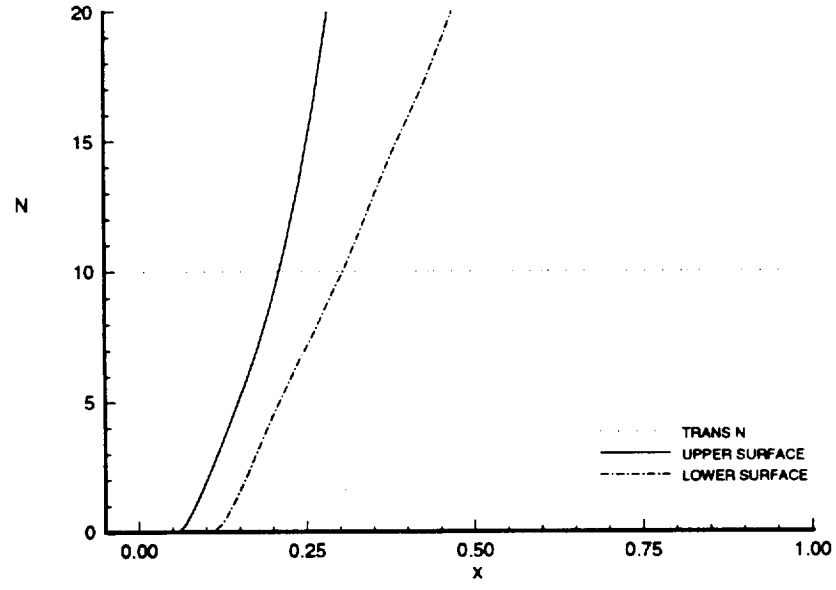

Figure 23. The upper and lower surface N-Factor distributions of the NACA 1412 airfoil at $M_\infty = 0.60$, $Re = 20$ million, and $c_l = 0.40$

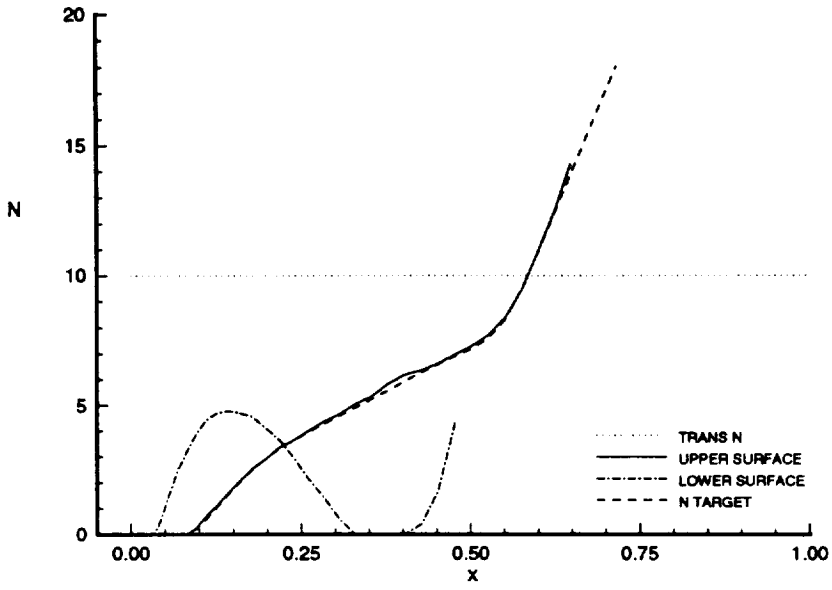

Figure 24. The upper and lower surface N-Factor distributions of the redesigned NACA 1412 airfoil at $M_\infty = 0.60$, $Re = 20$ million, and $c_l = 0.40$

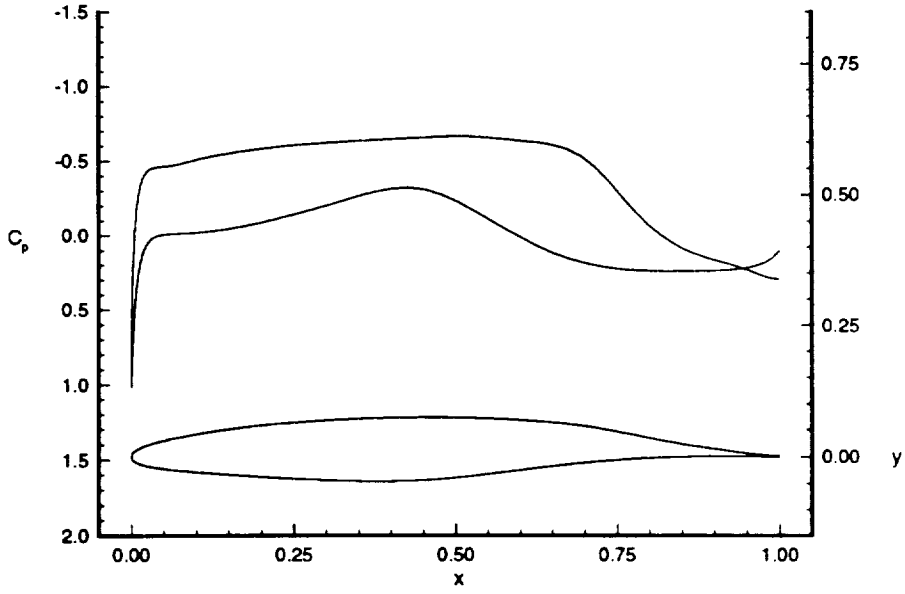

Figure 25. The pressure distribution and shape of the redesigned NACA 1412 airfoil at $M_\infty = 0.60$, $Re = 20$ million, and $c_l = 0.40$

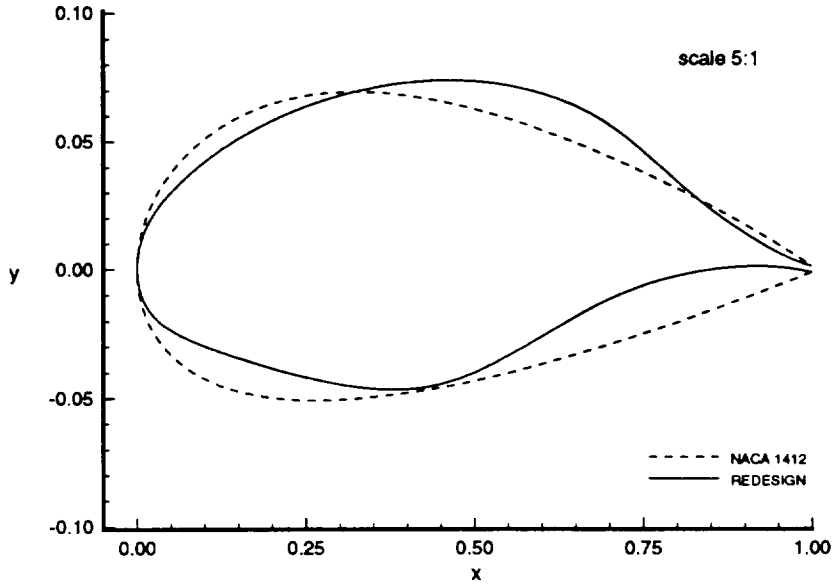

Figure 26. A comparison of the NACA 1412 airfoil and the redesigned NACA 1412 airfoil

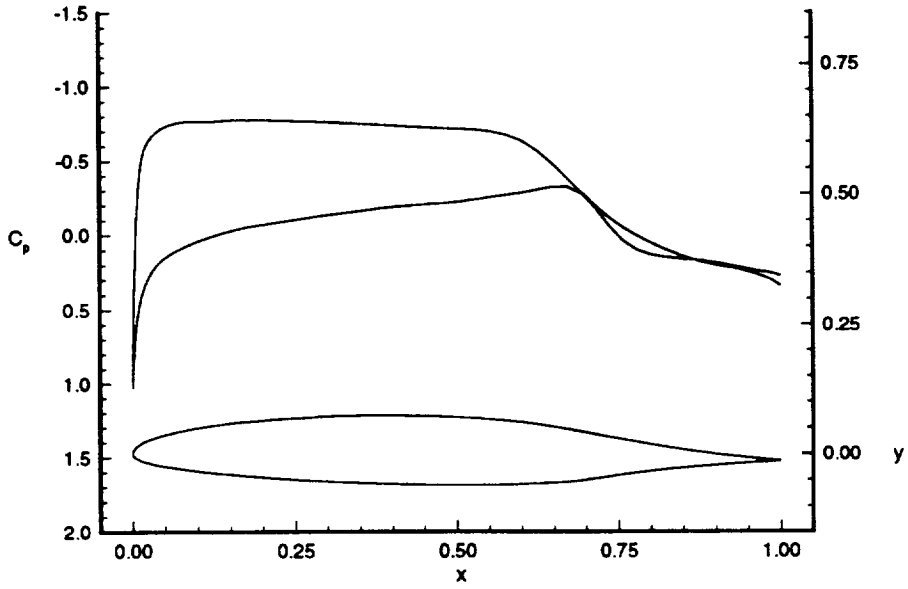

Figure 27. The pressure distribution and shape of the NASA High Speed NLF-0213 airfoil at $M_\infty = 0.60$, $Re = 20$ million, and $c_l = 0.40$

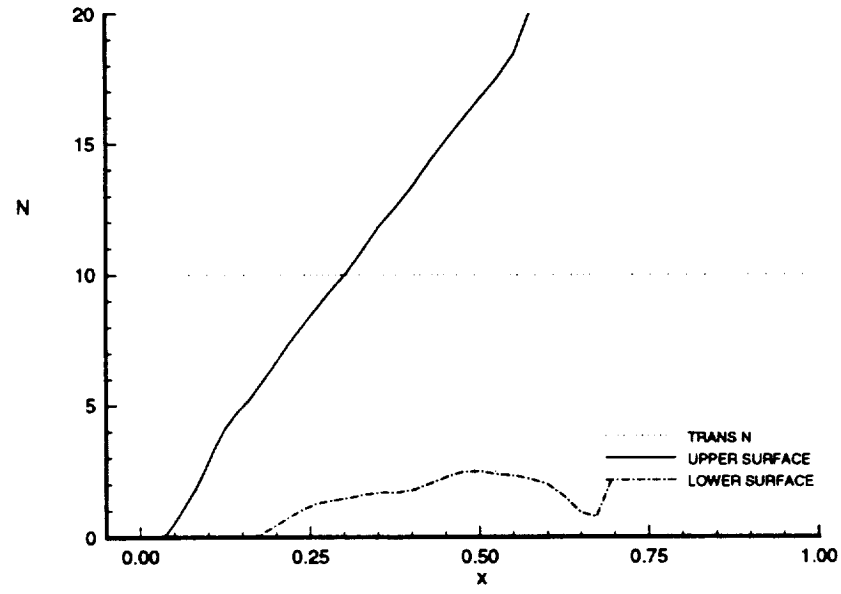

Figure 28. The upper and lower surface N-Factor distributions of the NASA High Speed NLF-0213 airfoil at $M_\infty = 0.60$, $Re = 20$ million, and $c_l = 0.40$

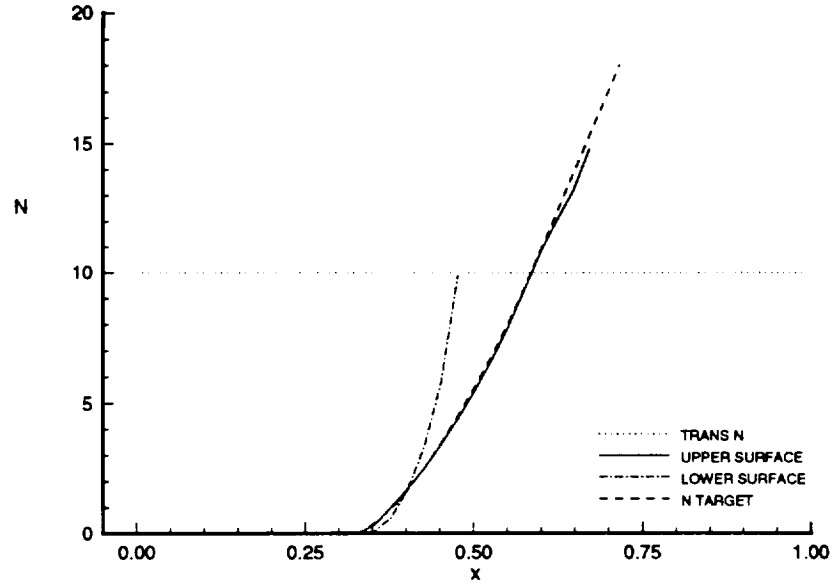

Figure 29. The upper and lower surface N-Factor distributions of the redesigned NLF-0213 airfoil at $M_\infty = 0.60$, $Re = 20$ million, and $c_l = 0.40$

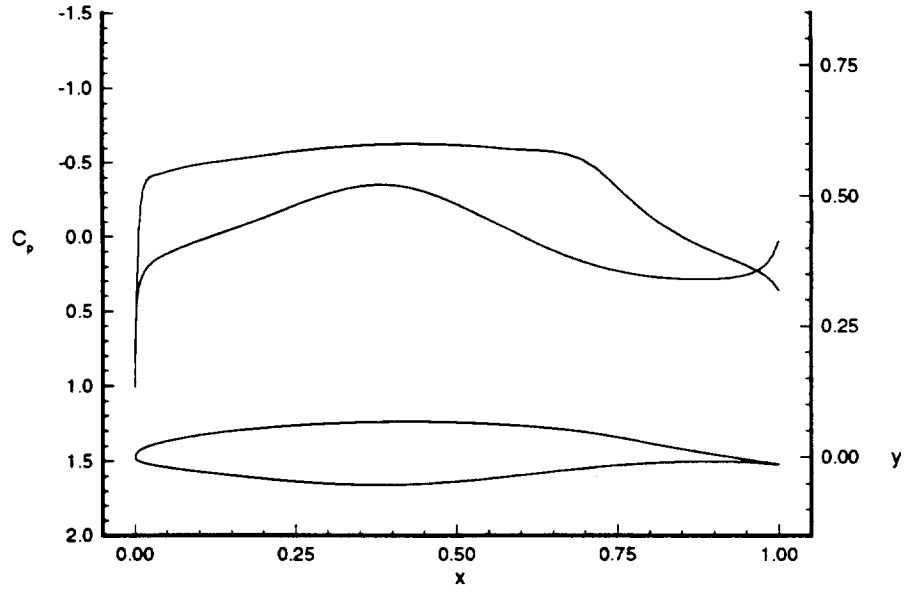

Figure 30. The pressure distribution and shape of the redesigned NLF-0213 airfoil at $M_\infty = 0.60$, $Re = 20$ million, and $c_l = 0.40$

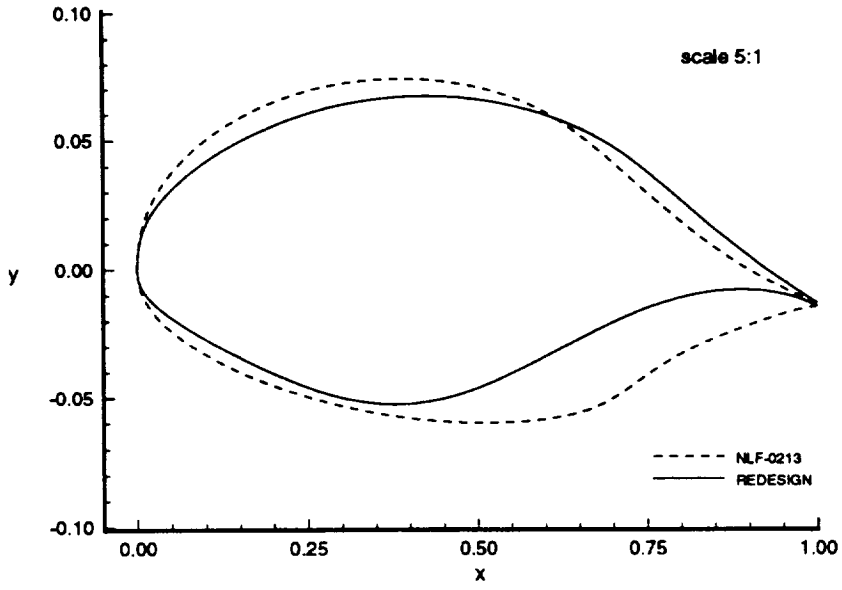

Figure 31. A comparison of the NASA High Speed NLF-0213 airfoil and the redesigned NLF-0213 airfoil

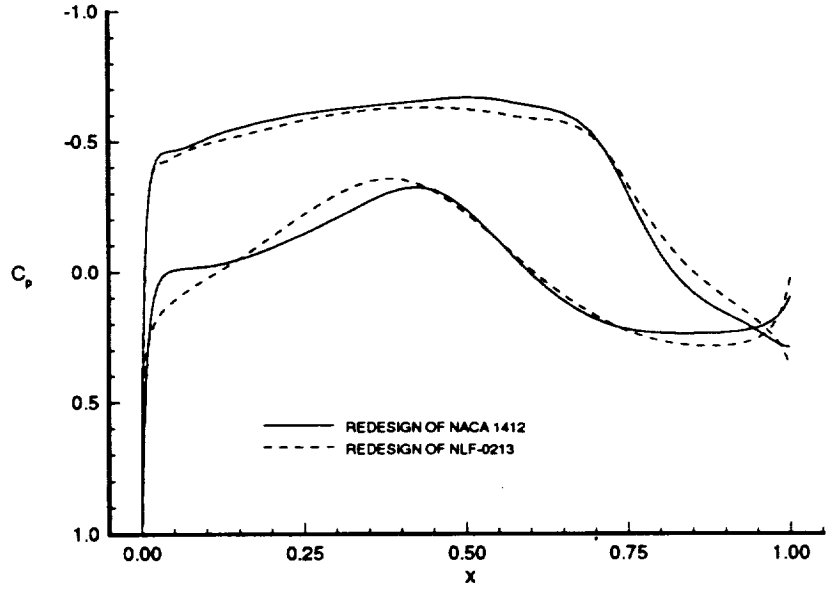

Figure 32. A comparison of the pressure distributions of the redesigned NACA 1412 airfoil (Figure 25) and the redesigned NASA High Speed NLF-0213 airfoil (Figure 30)

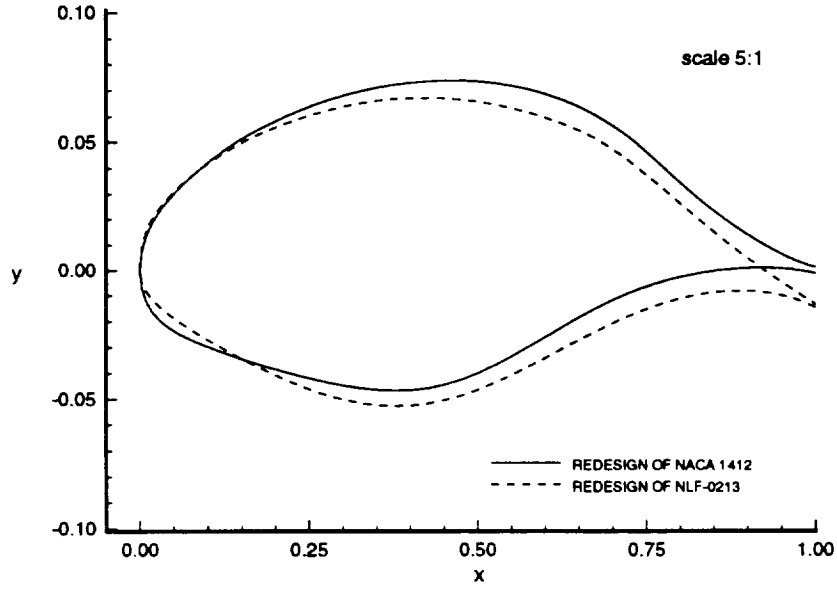

Figure 33. A comparison of the redesigned NACA 1412 airfoil (Figure 25) and the redesigned NASA High Speed NLF-0213 airfoil (Figure 30)

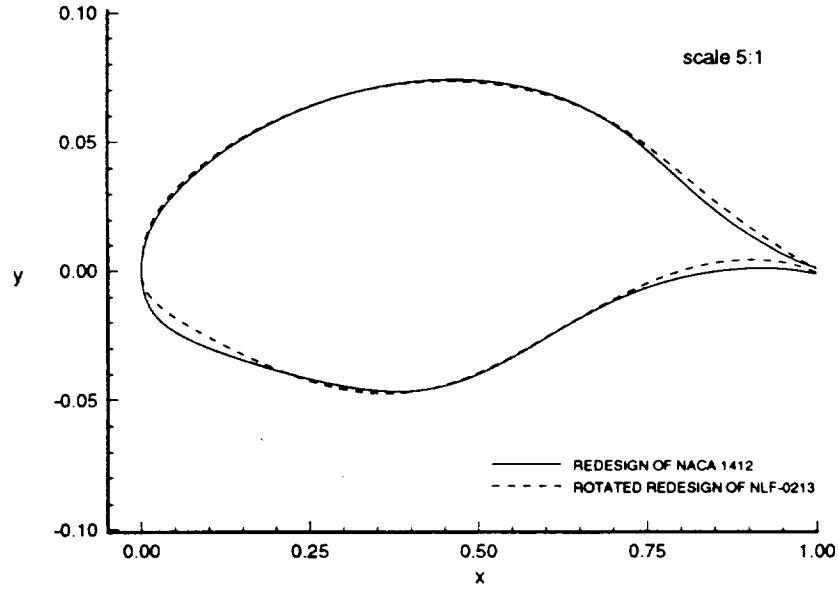

Figure 34. A comparison of the redesigned NACA 1412 airfoil and the redesigned NASA High Speed NLF-0213 airfoil after rotation

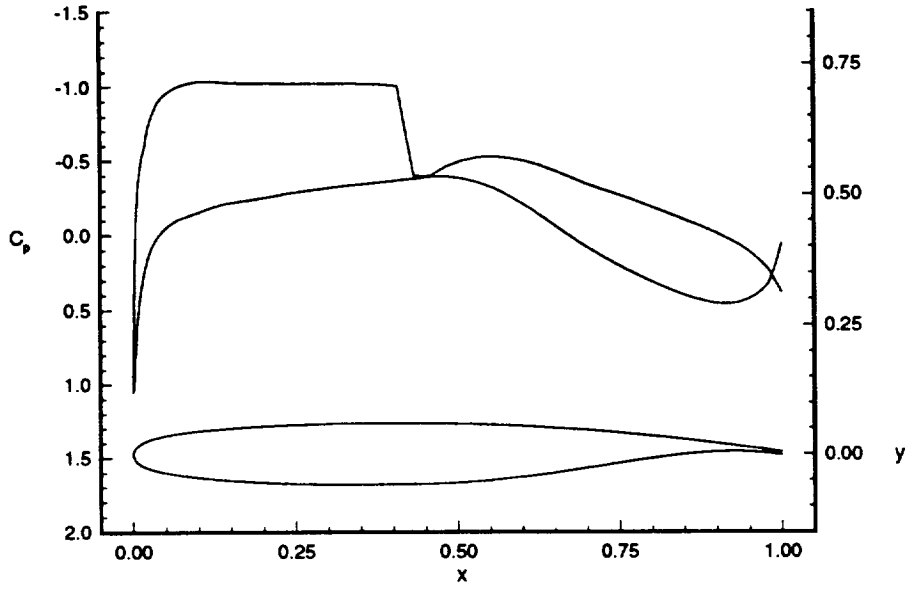

Figure 35. The pressure distribution and shape of the NASA Supercritical SC(2)-0412 airfoil at $M_\infty = 0.76$, $Re = 10$ million, and $c_l = 0.50$

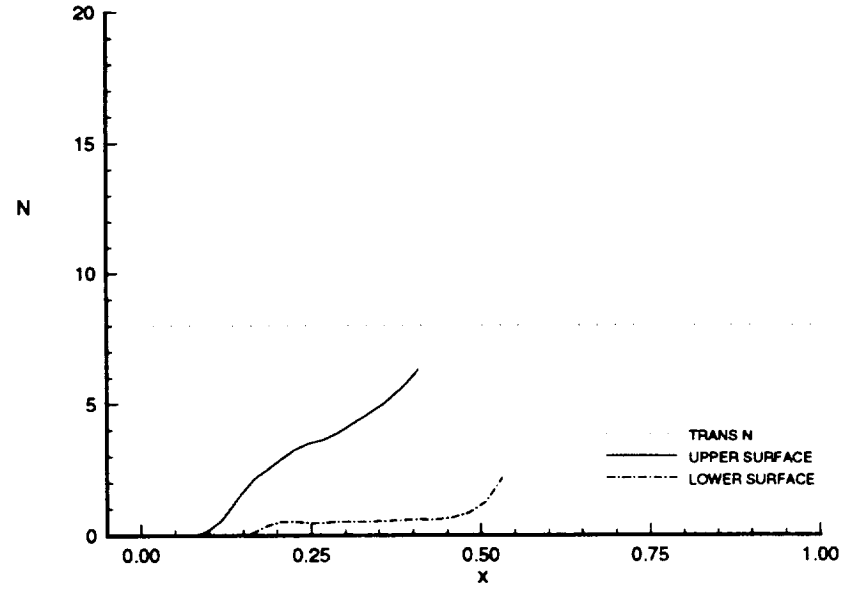

Figure 36. The upper and lower surface N-Factor distributions of the NASA Supercritical SC(2)-0412 airfoil at $M_\infty = 0.76$, $Re = 10$ million, and $c_l = 0.50$

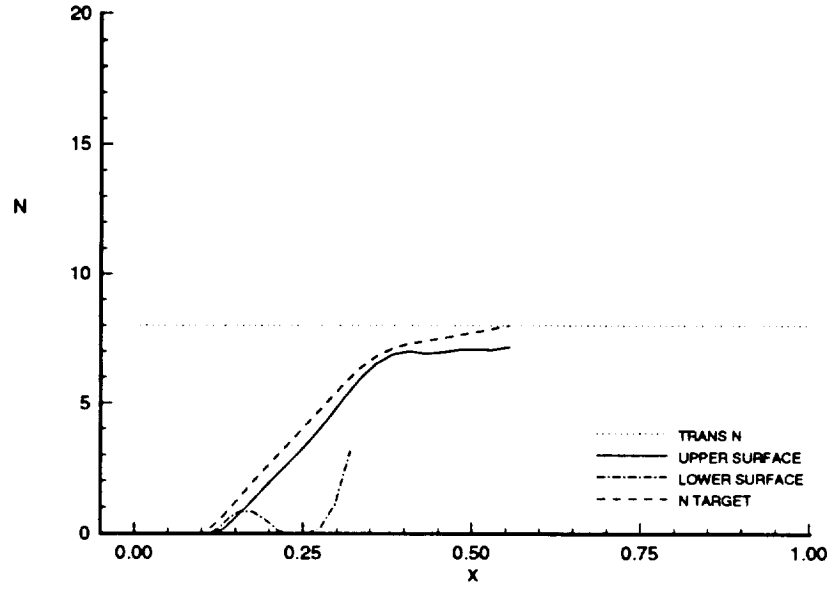

Figure 37. The upper and lower surface N-Factor distributions of the redesigned SC(2)-0412 airfoil at $M_\infty = 0.76$, $Re = 10$ million, and $c_l = 0.50$

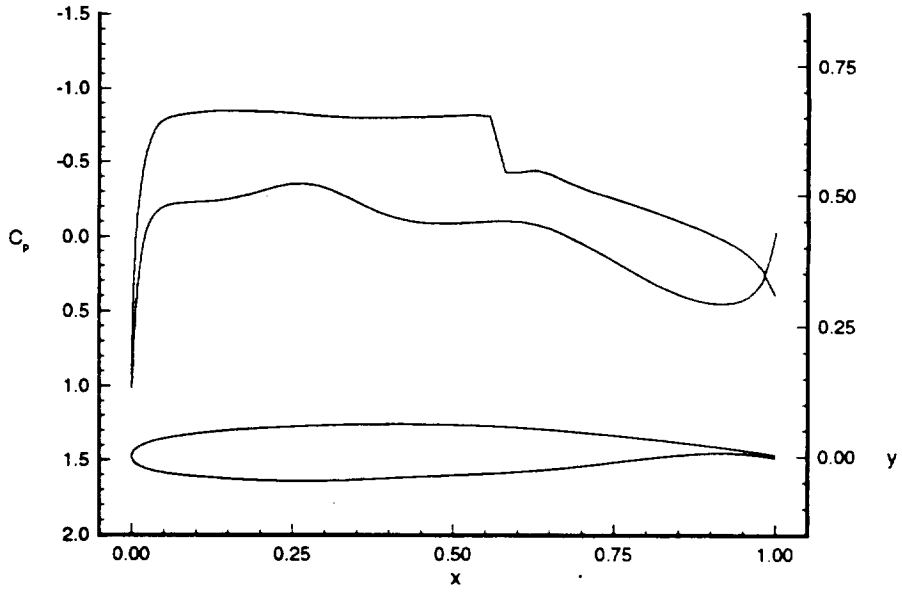

Figure 38. The pressure distribution and shape of the redesigned SC(2)-0412 airfoil at $M_\infty = 0.76$, $Re = 10$ million, and $c_l = 0.50$

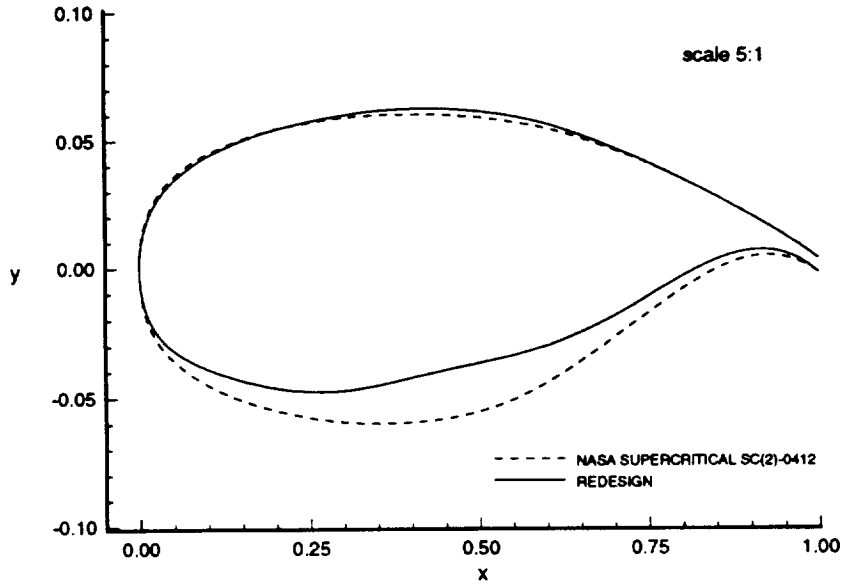

Figure 39. A comparison of the NASA Supercritical SC(2)-0412 airfoil and the redesigned SC(2)-0412 airfoil

Appendix A. A Linear Scaling Method

In a few cases within the NLF airfoil design method, it is desirable to calculate a new target pressure distribution that has nearly the same shape as another pressure distribution, but different pressure magnitudes. This can be accomplished by linearly scaling an existing pressure distribution. Consider the pressure distribution shown in Figure A.1. Suppose that this pressure distribution, $C_{p,j}$, is to be linearly scaled to obtain a new target pressure distribution. In addition, assume that the pressure coefficient at 50% chord of the new target pressures is to be -0.30, while the leading-edge pressure coefficient is to remain unchanged. The new target pressures can be calculated using the relation

$$C_{p,T,j} = (C_{p,j} - C_{p,1})\,G + C_{p,1} \tag{A.1}$$

where G is the scale factor and $C_{p,1}$ represents the leading-edge pressure coefficient of $C_{p,j}$. In this case,

$$G = \frac{-0.30 - C_{p,1}}{C_{p,k} - C_{p,1}} \tag{A.2}$$

where k represents the station nearest to 50% chord. Notice that when Equations A.1 and A.2 are used, $C_{p,T,1} = C_{p,1}$ and $C_{p,T,k} = -0.30$ as desired. The new target pressure distribution that results from using Equations A.1 and A.2 is shown in Figure A.2.

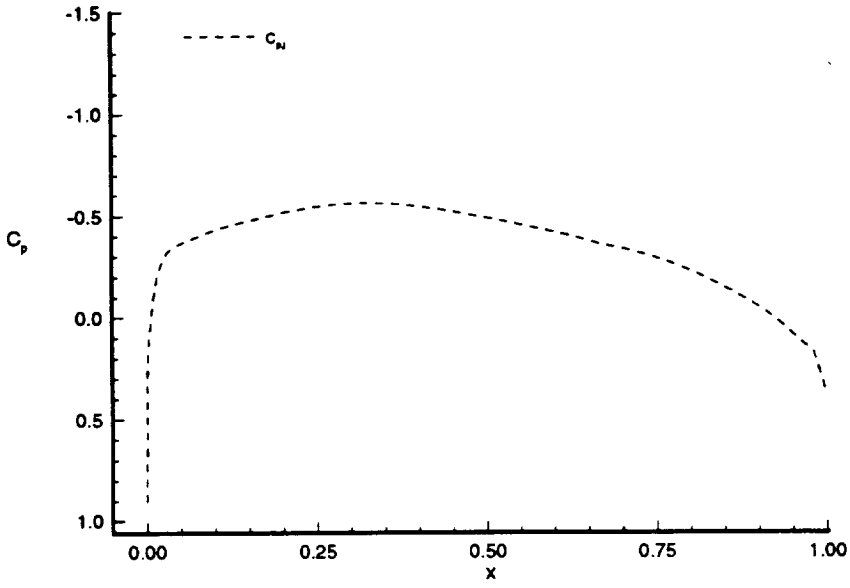

Figure A.1. The pressure distribution used to calculate the new target pressures

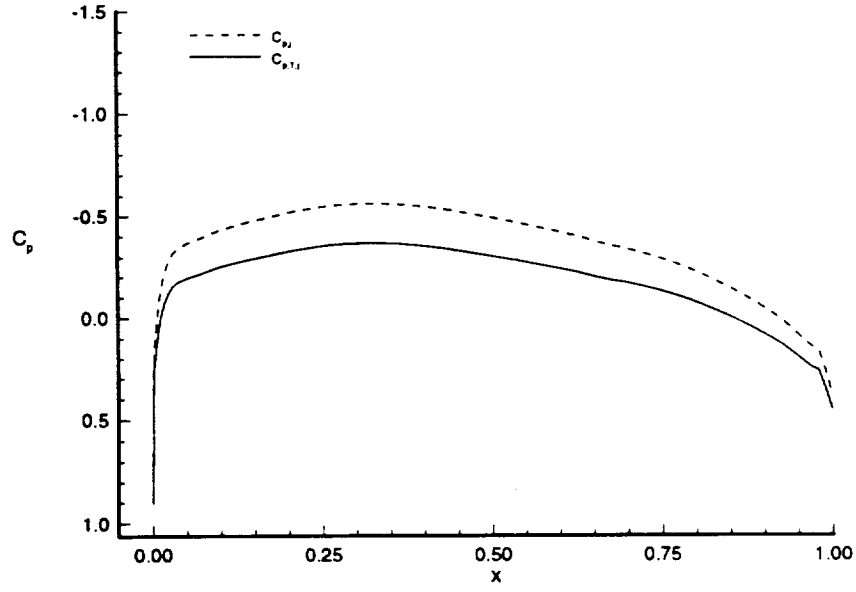

Figure A.2. The new target pressure distribution that results from using a linear scaling technique

Appendix B. A Weighted Averaging Technique

On several instances within the NLF airfoil design method, a weighted averaging technique is used to calculate a new target pressure distribution from two existing pressure distributions. This weighted averaging technique calculates a new target pressure distribution using the relation

$$C_{p,T,j} = W_j C_{p,j,1} + (1 - W_j) C_{p,j,2} \tag{B.1}$$

where W_j is a weighting function, and $C_{p,j,1}$ and $C_{p,j,2}$ are two existing pressure distributions. A similar weighted averaging technique is used in reference 29.

In the NLF airfoil design method, Equation B.1 is most useful when W_j is allowed to vary along the chord since it is usually desirable to maintain certain characteristics of each of the two existing pressure distributions. Consider the two pressure distributions shown in Figure B.1. Suppose that these two distributions are to be used to calculate a new target pressure distribution, and that the leading-edge pressures of $C_{p,j,1}$ and the trailing-edge pressures of $C_{p,j,2}$ are to be retained as the target pressures in each of the respective regions. If W_j is allowed to vary from a value of 1 at the leading-edge to a value of 0 at the trailing-edge, it can be seen from Equation B.1 that the resulting target pressures would have the desired properties in the leading-edge and trailing-edge regions.

The simplest expression for W_j that satisfies these requirements would be a linear variation between the leading-edge and the trailing-edge. That is,

$$W_j = 1 - x_j \tag{B.2}$$

Figure B.2 shows the new target pressures that result from using $C_{p,j,1}$ and $C_{p,j,2}$ from Figure B.1 and the weighting function from Equation B.2.

Equation B.1 can also be used to modify the target pressures over only a small region of the chord. In fact, this is the only application of the technique that is used within the NLF airfoil design method. Suppose that $C_{p,j,1}$ represents the current target pressures and $C_{p,j,2}$ represents the current analysis pressures. It may be desirable to retain the target pressures of $C_{p,j,1}$ ahead of 60% chord (i.e., $W_j = 1$ ahead of 60% chord), but, at the same time, retain the characteristics of $C_{p,j,2}$ at the trailing-edge. If station k represents the ordinate closest to 60% chord, then W_j can be varied linearly from a value of 1 at station k to a value of 0 at the trailing-edge. As a result, the weighting function aft of 60% chord can be represented by the expression

$$W_j = \frac{1 - x_j}{1 - x_k} \tag{B.3}$$

The target pressure distribution that results from using Equation B.1 is shown in Figure B.3.

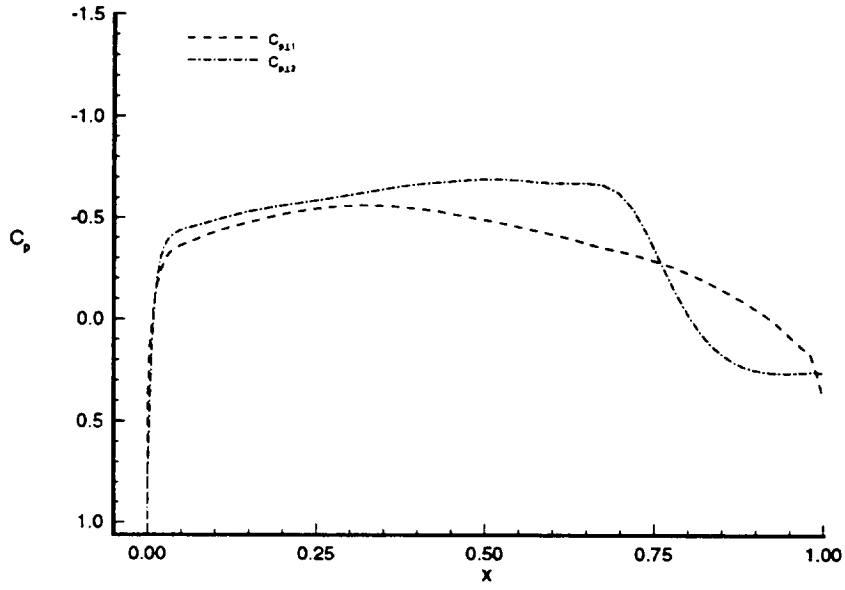

Figure B.1. Two existing pressure distributions

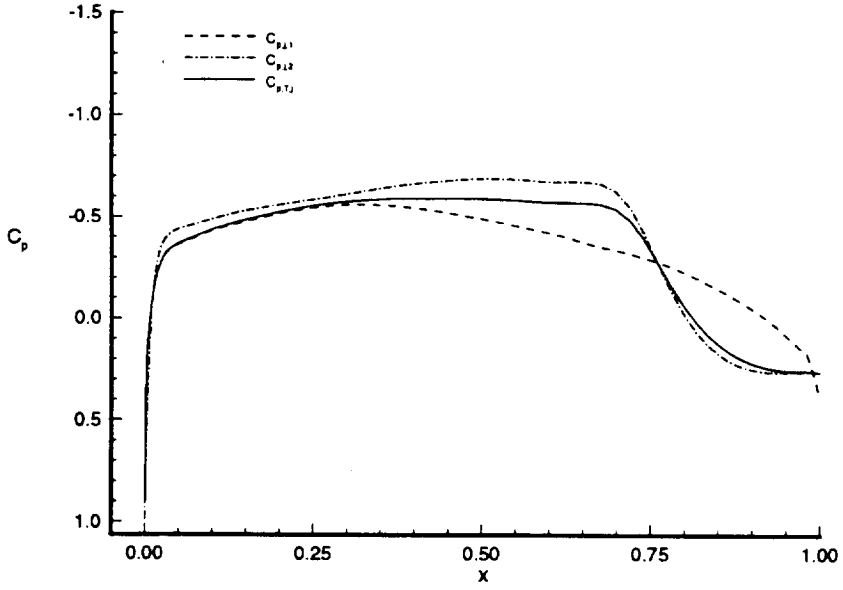

Figure B.2. The new target pressure distribution obtained by using a weighting function over the entire length of the chord

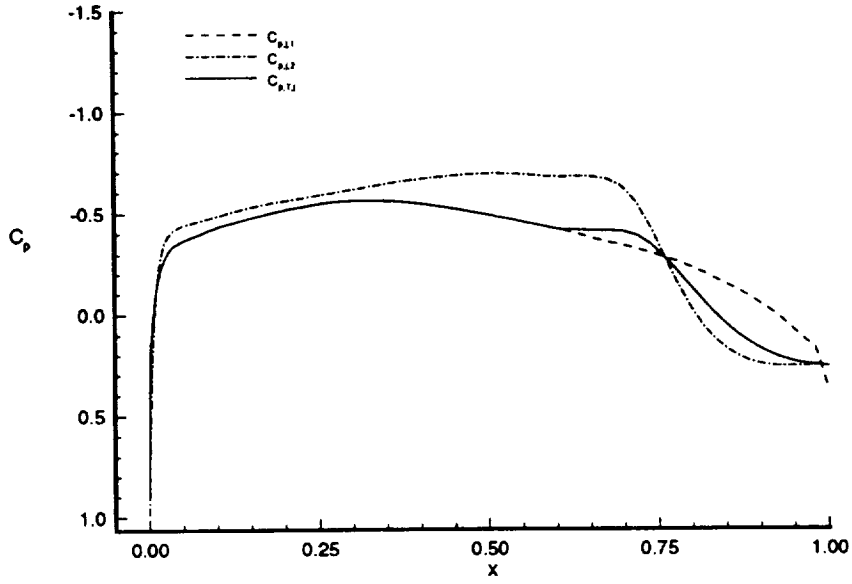

Figure B.3. The new target pressure distribution obtained by using a weighting function over a small region of the chord